NATIONAL ADVISORY COMMITTEE FOR AERONAUTICS

WARTIME REPORT

ORIGINALLY ISSUED

March 1944 as
Memorandum Report

FORCE TESTS OF A 1/5-SCALE MODEL OF THE

TYPE GB-5 CONTROLLABLE GLIDE BOMB

By Marvin Pitkin

Langley Memorial Aeronautical Laboratory
Langley Field, Va.

NACA

WASHINGTON

NATIONAL ADVISORY COMMITTEE FOR AERONAUTICS

MEMORANDUM REPORT

for the

Army Air Forces, Materiel Command

FORCE TESTS OF A 1/5-SCALE MODEL OF THE

TYPE GB-5 CONTROLLABLE GLIDE BOMB

By Marvin Pitkin

INTRODUCTION

At the request of the Army Air Forces, Materiel
Command, the NACA is assisting in the development of
a type GB-5 controllable glide bomb equipped with a
"target-seeking" device. In order to measure the
stability and control characteristics of the bomb in
its original condition and with various modifications
a 1/5-scale model has been tested on the six-component
balance in the free-flight tunnel. The tests included
the development of suitable means for altering the
effective dihedral and the directional stability by
simple structural modifications, the development of a
device capable of altering the lift-drag ratio of the
bomb without changing the angle of attack, and the
measurement of the rolling- and yawing-moment charac-
teristics of the ailerons. The results of these tests
are presented herein.

Force tests were made for 12 different vertical-
tail configurations and the effect of six different
sets of wing-tip end plates upon the effective dihedral
characteristics of the model was studied. The influence
of two sets of spoilers, two sets of double-split
rudders, one set of double-split flaps, and five sets
of split flaps upon the lift-drag characteristics of
the model was investigated and the characteristics of
the beveled-nose, plain-flap-type ailerons were obtained.
Most of the tests were made at an angle of attack of 8°
which corresponded to the launching angle of the full-
scale bomb.

SYMBOLS

α angle of attack of bomb center line, degrees

ψ angle of yaw, degrees

C_L lift coefficient $\dfrac{\text{Lift}}{\frac{\rho}{2}SV^2}$

C_D drag coefficient $\dfrac{\text{Drag}}{\frac{\rho}{2}SV^2}$

C_m pitching-moment coefficient $\dfrac{\text{Pitching moment}}{\frac{\rho}{2}SV^2 c}$

C_l rolling-moment coefficient $\dfrac{\text{Rolling moment}}{\frac{\rho}{2}SV^2 b}$

C_Y lateral-force coefficient $\dfrac{\text{Lateral force}}{\frac{\rho}{2}SV^2}$

C_n yawing-moment coefficient $\dfrac{\text{Yawing moment}}{\frac{\rho}{2}SV^2 b}$

C_{l_ψ} effective-dihedral parameter, rate of change of rolling-moment coefficient with angle of yaw $\left(\dfrac{dC_l}{d\psi}\right)$

C_{n_ψ} directional-stability parameter, rate of change of yawing-moment coefficient with angle of yaw $\left(\dfrac{dC_n}{d\psi}\right)$

L/D lift over drag ratio

ρ density of air, slugs per cubic foot

S wing area, square feet

V true airspeed, feet per second

b wing span, feet

c wing chord, feet

δ   control deflection, degrees, with subscripts as
          follows:

        f   flap

        e   elevator

        r   rudder

        a   aileron

APPARATUS AND METHODS

Wind tunnel.- The tests were made in the free-
flight tunnel, a complete description of which is given
in reference 1. The free-flight-tunnel balance, upon
which the tests were made, is a six-component balance
which so rotates with the model in yaw that all forces
and moments are measured with respect to the stability
axes. A photograph of the 1/5-scale model of the glide
bomb mounted inverted on this balance is given in fig-
ure 1. A more complete description of this balance and
its operation is given in reference 2.

Model.- The model was supplied by the Materiel
Command, Army Air Forces and was prepared for balance
testing by the installation of a standard mounting plate
used to attach models to the balance strut. A three-
view drawing of the model is given in figure 2. Photo-
graphs of the model as it was originally received are
shown in figure 3.

Sketches of the wing-tip end plates used in the
tests are presented in figure 4 and sketches of the
various vertical tails tested are given in figures 5
and 6. The aileron system tested is also shown in
figure 6. Figure 7 shows sketches of the various glide-
path controls investigated in the tests.

Test conditions.- All of the force tests were run
at a dynamic pressure of 4.09 pounds per square foot
which corresponds to an airspeed of about 40 miles per
hour at standard sea-level conditions and to a test
Reynolds number of 204,000 based on the mean chord of
0.55 foot. The moments and forces measured on the

balance were transferred to the center-of-gravity loca-
tion below the 25-percent chord line at a distance
6-percent chord above the center line of the bomb.

TEST PROCEDURE

The test program was so laid out that all of the
stability changes could be obtained by simple structural
modification of the glide bomb. This limitation was
deemed necessary in order to permit full use to be made
of full-scale bomb units already manufactured. A
preliminary analysis of the stability requirements for
a controlled glide bomb indicated the desirability of
being able to obtain a range of values of the effective-
dihedral parameter C_{l_ψ}, and the directional-stability

parameter C_{n_ψ} from the values for the bomb as ori-

ginally received down to zero. The test program was
laid out, therefore, in such a manner that any desired
values of these stability parameters could be obtained
by a selection of the proper end plates and vertical
tail size. A special effort was made to find a combina-
tion of surfaces that would yield a value of C_{l_ψ} of

0.00030 and C_{n_ψ} of -0.00018 because calculations had

indicated that this combination of derivatives might
yield good flight characteristics with a rudder control.

The directional stability of the bomb was reduced
by two different methods. One was the reduction of area
on the existing tail booms and was accomplished simply
by removing one of the tails or by removing portions
from the top and bottom of the tails, keeping the chord
constant, as shown in figure 5, to form tails 1 to 11.
The second method was the addition of tail area on
forward booms to form tail 12 on figure 6. This arrange-
ment was tested because it would result in greater
damping in yaw.

For each vertical-tail and end-plate arrangement,
the rolling moment, yawing moment, and lateral force
due to yaw were determined.

The rolling and yawing moments produced by the
ailerons were measured for the right aileron alone

deflected up and down various amounts. The moments for simultaneous deflection of both ailerons may be obtained by summation of the moments for the up and the down deflections.

The goal of the glide-path control tests was to develop a device which would change the L/D ratio from 7 to 0 without altering a given angle of attack or elevator setting. A further proviso was that it should be possible for some setting of this device to obtain a lift coefficient of 0.64, a condition corresponding to the most suitable launching speed of the bomb. Although it was obvious that only lift-decreasing devices could reduce the L/D ratio to zero, tests were made of several devices operating wholly on drag-increasing principles in the hope that their simplicity of operation would offset their inability to produce an L/D ratio of zero.

RESULTS AND DISCUSSION

Effect of End Plates on Dihedral Parameter

The use of vertical end-plate area butted to the ends of the wings as shown in figure 4 was found to be an effective and simple means of altering the dihedral parameter C_{l_ψ}. The effect of end plates 1, 3, 4, and 5, which extended wholly below the lower surface of the wing, upon the static lateral-stability characteristics, is shown in figure 8 and the variations of C_{l_ψ} with vertical end-plate area are summarized in figure 9. These data indicate that the effective-dihedral parameter C_{l_ψ} was reduced almost directly proportionally to the amount of vertical area added below the wing at the wing tip. The action of the vertical end plates in reducing the effective dihedral must be entirely ascribed to the restrictions imposed by these areas upon the cross-flow conditions around the wing tips. This was indicated by calculations which showed that the rolling-moment contribution of the end plates as isolated aerodynamic surfaces was not only very small but was such as to increase the effective dihedral because the resultant center of pressure of the aerodynamic loads on the end plates tested is above the center of gravity.

The action of the upper-surface end plates 2 upon the effective-dihedral parameter C_{l_ψ} is shown in figure 10. These data indicate that adding end-plate area above the surface of the wing acts oppositely to adding area below the wing and consequently increased C_{l_ψ}. The large reduction of C_{l_ψ} initially caused by lower-surface end plates 1 was almost completely nullified by the addition of the smaller end-plate surfaces 2.

Effect of Vertical-Tail Arrangement

Upon Directional Stability

The effect of the twin-tail designs 1 through 4 upon the lateral-stability characteristics of the model at 8° angle of attack are shown in figure 11. The results of the tests conducted with the asymmetrically located single-vertical tail designs 5 through 8 are presented in figure 12. Although the lateral-force and yawing-moment data presented in figures 11 and 12 are consistent, the rolling-moment data of these figures are erratic and do not agree with the corresponding data of the no-end-plate run of figure 8 which were obtained at 6° angle of attack. The rolling-moment data of figures 11 and 12 were believed erratic because of premature wing stalling caused by the low scale of the tests; therefore, the remaining directional-stability tests were conducted chiefly at an angle of attack of 6°. The results of figure 12 also indicated that the single-tail designs caused unsymmetrical yawing-moment characteristics with yaw and, hence, would cause unsatisfactory flight behavior. This point is illustrated in figure 13 in which are presented yawing-moment data for twin tails and for tails located on the left or right of the stabilizer.

The results of figures 11 and 12 are summarized in figure 14 in which is shown the variation of the directional-stability parameter, C_{n_ψ} with vertical-tail area aft of the center of gravity. These data indicated that a twin-tail design of three-eighths the area of tail 1 would probably create the desired value of C_{n_ψ} of -0.00018. The results of tests made with

a vertical tail of this size (tail 11) and with lower end plates 6 are shown in figure 15. These end plates were selected on the basis of the results presented in figure 9 which indicated that the end plates of 18.5-percent wing area would provide the desired value of C_{l_ψ} of 0.00030. The results of figure 15 indicate that the desired specifications for C_{n_ψ} and C_{l_ψ} were met at $6°$ angle of attack with these vertical tails and end plates installed.

The variation of the lateral-stability characteristics with angle of attack of the model equipped with end plates 6 and vertical tails 11 is shown in figure 16. These results indicated that there was considerable variation of C_{n_ψ} with angle of attack and that when the specified value of C_{n_ψ} was obtained at $6°$ angle of attack, the value of C_{n_ψ} was too large at the required angle of attack of $8°$. It was further indicated that directional instability would occur at smaller angles of attack and that, if the vertical-tail area was further reduced to yield the required degree of directional stability at $8°$ angle of attack, the bomb would then be directionally unstable over most of the low angle-of-attack range.

It was believed that the variation of C_{n_ψ} with angle of attack of the bomb arose due to wing characteristics inasmuch as the results of reference 3 indicated similar variations of C_{n_ψ} with angle of attack for rectangular wings. Additional tests were therefore run to check this point. For these tests the characteristics of the model as originally received (tail 1, no end plates) were investigated over the angle-of-attack range. The results of these tests are plotted in figure 17 and are summarized with the data of figures 15 and 16 in figure 18. Data for an isolated rectangular wing, obtained from reference 3, are also shown in figure 18 for purposes of comparison.

The results of figure 18 indicate that the increase in directional stability with increased angle of attack is independent of tail design and, therefore, must be primarily a wing characteristic. It appears, therefore, that the desired degree of directional stability cannot

be achieved at 8° angle of attack without resulting in directional instability at angles of attack smaller than 8°. This conclusion was further substantiated by tests of forward tails 12 acting together with the original tails 1 - a configuration shown in figure 6.

The static lateral-stability characteristics of the model equipped with the original vertical tails 1 and forward tails 12 are presented in figure 19. These data indicate that the directional stability of the model at 8° angle of attack was just barely stable. The results of figure 19 are summarized in figure 20 and show the same variation of directional stability with angle of attack previously noted. The data indicated that the model with the coupled tail arrangement would be directionally unstable at angles of attack smaller than 8°.

Aileron Tests

The data from tests of the aileron system shown in figure 6 are presented in figure 21 at various angles of attack for the right aileron alone deflected various amounts from 15° up to 15° down.

Glide-Path Control

In order to provide the data necessary to convert pitching moments to elevator deflections required to trim at a given angle of attack, tests were run of the model with elevator set at 0° and ±10°. The results of these tests are presented in figure 22.

Spoilers.- Tests were run to determine the effect of the upper-surface spoilers shown in figure 7, inasmuch as this type of device both decreases lift and increases drag. The results of these tests are shown in figure 23. These data show that although spoilers of 39 percent of the span decreased the L/D ratio at the angle of attack corresponding to $C_L = 0.64$ from 7.0 to 2.9 a further increase in spoiler span of 22 percent span only decreased the L/D ratio to 2.5, a value deemed unsatisfactory. In addition, both inboard and outboard spoilers created large diving moments, particularly inboard spoilers 1, and consequently required rather large changes in elevator deflection to maintain constant angle of attack.

The large diving moments encountered with spoilers 1 were believed to be primarily caused by the influence of the decreased wing downwash upon the tail surfaces immediately behind.

Double-split rudders.- Figure 24 presents the effect of double-split rudders A (mounted on end plates 4 as shown in figure 4) on the aerodynamic characteristics of the model. The data on figure 24 were rearranged in conjunction with the elevator data given in figure 22 to show the variation of L/D ratio, C_L, and elevator angle required to trim with rudder deflection and are thus presented in figure 25. These data are given for the angle of attack $8°$ at which it was possible to approach the specified value of lift coefficient of 0.64.

The data presented in figures 24 and 25 indicate that the double-split rudder A was inadequate as a glide-path control device and would merely alter the L/D ratio from 7.7 to 4.1 for full rudder deflection ($±60°$). A further attempt was made to lower the L/D ratio by use of split rudders of greater span than rudders A. The results of tests made with double-split rudders B mounted on end plate 3 are shown in figures 26 and 27. Although rudders B were twice the span of rudders A, they reduced the L/D ratio only a slight amount further and consequently no other tests were made utilizing the double-split-rudder type of controls. It is interesting to note that both rudders A and particularly rudders B increased the lift on the wing - thereby emphasizing the critical nature of air-flow conditions about the wing tips.

Double-split flaps.- Tests were made of double-split flaps A extending over the outboard 42 percent of the wing span as shown in figure 7. The results of these tests are plotted similarly to those of the rudder tests and are presented in figures 28 and 29. The results presented in figure 29 show that the double-split flaps deflected 60° up and down decreased the L/D ratio from 7.3 to 2.1. This decrease, although considerable, was still not considered sufficient. In addition, a considerable change in elevator angle was required to trim at a constant angle of attack.

Lower-surface split flaps.- Figures 20 and 31 show the effect of a lower-surface split flap 1 of 42-percent

span located as shown in figure 7. These data show a fairly small variation of L/D ratio with downwardly deflected flaps. The data from these tests indicated that the diving moments caused by the flaps on the wing were almost wholly nullified on the complete model. This action undoubtedly arose owing to the effects of the increased wing downwash on the pitching moments contributed by the horizontal tail surfaces.

Upper-surface split flaps.- The tests of lower-surface flaps 1 indicated that upper-surface flaps would be required to alter the L/D ratio as desired. It was also indicated from those tests and from the spoiler tests previously discussed that the upwash effects of the upper-surface flaps upon the horizontal tail could be employed to nullify the incremental wing moments caused by flap deflection. Such configuration would then alter the L/D ratio without changing the angle of attack or elevator angle. In order to determine the proper flap arrangement and location, tests were first made of split flaps 2 which are identical with flap 1 but are mounted on the upper wing surface over the inboard 42 percent of the wing span. The results of these tests are presented in figures 32 and 33 and indicate that flaps 2 came very close to meeting all specifications. Only a slight amount of elevator adjustment was required to trim and the L/D ratio at 0° angle of attack was reduced from 7.3 to 1.3 for 60° flap deflection.

In order to reduce the L/D ratio still further, the span of flap 2 was increased to 50-percent wing span to form flaps 3. The results of the tests of flap 3 are presented in figures 34 and 35. Although the results presented in these figures indicated that flap 3 would satisfactorily reduce the L/D ratio to zero as desired, a large increment of up elevator was required to trim out the pitching moments caused by flap deflection.

It appeared likely that the diving moments arising from deflection of flap 3 were caused by downwash changes on the horizontal tail such that the tail moments over-balanced the wing stalling moments created by flap deflection. In order to assist in finding the spanwise location of a flap, which required no change in elevator settings when deflected, further tests were run in which flap 3 was moved to the outboard portion of the wing. The results of tests made with the flap in this position

(flap 4) are presented in figures 36 and 37. These results indicated that with this arrangement a large increment of down elevator would be required to trim out the moments due to flap deflections.

A study of the results of the tests of flaps 3 and 4 indicated that a 60-percent span flap located at the center of each wing panel should provide the desired L/D control without requiring large elevator changes to maintain a constant angle of attack. The results of such a flap (flap 5) are presented in figures 38 and 39 and substantiate this belief. These data indicate that it is possible to secure a reduction in L/D ratio with flap 5 from 7.2 to 0 with only 3° elevator-deflection change being required to maintain the desired angle of attack (8°). It appears that even this slight change of elevator deflection could be eliminated by the expedient of moving flap 5 a slight amount inboard.

CONCLUDING REMARKS

Force tests of a 1/5-scale model of a type GB-5 controllable glide bomb in the NACA free-flight tunnel indicated the following:

1. The effective-dihedral characteristics of the model were widely varied by the addition of vertical end plates butted to the wing tips. Addition of end-plate area below the wing surface reduced the effective dihedral whereas area added above the wing increased the effective dihedral.

2. The model wing characteristics were such as to cause an increase in directional stability with increased angle of attack. This change in directional stability with angle of attack was independent of vertical-tail design. Consequently, a moderately large amount of directional stability was required at low speed to avoid directional instability over the high-speed portion of the speed range.

3. Upper-surface, upwardly deflected, split flaps located at the center of each wing panel reduced the lift over drag ratio from 7.2 to 0 without appreciably changing the angle of attack (8°).

Langley Memorial Aeronautical Laboratory,
    National Advisory Committee for Aeronautics,
        Langley Field, Va., March 27, 1944.

Marvin Pitkin,
Aeronautical Engineer.

Approved:

Hartley A. Soulé,
Chief of Stability Research Division.

ES

REFERENCES

1. Shortal, Joseph A., and Osterhout, Clayton J.: Preliminary Stability and Control Tests in the NACA Free-Flight Wind Tunnel and Correlation with Full-Scale Flight Tests. NACA TN No. 810, 1941.

2. Shortal, Joseph A., and Draper, John W.: Free-Flight-Tunnel Investigation of the Effect of the Fuselage Length and the Aspect Ratio and Size of the Vertical Tail on Lateral Stability and Control. NACA ARR No. 3D17, 1943.

3. Shortal, Joseph A.: Effect of Tip Shape and Dihedral on Lateral Stability Characteristics. NACA Rep. No. 548, 1935.

FIGURE LEGENDS

Figure 1.- Photograph of a $\frac{1}{5}$-scale model of the type
. GB-5 controllable glide bomb mounted inverted on the
free-flight tunnel balance strut.

Figure 2.- Three view sketch of the type GB-5 controllable
glide bomb as originally received. All dimensions are
in inches.

Figure 3.- Photographs of $\frac{1}{5}$-scale model of type GB-5
controllable glide bomb.

Figure 4.- Sketches of vertical wing-tip end plates tested
in the free-flight-tunnel investigation of a $\frac{1}{5}$-scale
model of the type GB-5 controllable glide bomb.

Figure 5.- Sketches of aft vertical tail surfaces
installed on a $\frac{1}{5}$-scale model of the type GB-5 control-
lable glide bomb tested in the free-flight tunnel.

Figure 6.- Sketch of forward fins and ailerons tested on
a $\frac{1}{5}$-scale model of the type GB-5 controllable glide
bomb in the free-flight tunnel.

Figure 7.- Sketches of glide-path controls tested in the
free-flight tunnel investigation of a $\frac{1}{5}$-scale model of
the type GB-5 controllable glide bomb.

Figure 7.- Continued.

Figure 8.- Effect of lower-surface wing-tip endplates on
the static lateral-stability characteristics of
a $\frac{1}{5}$-scale model of the type GB-5 controllable glide
bomb. $\alpha = 6^{\circ}$; $\delta_e = \delta_r = \delta_f = \delta_a = 0^{\circ}$.

Figure 9.- Effect of lower-surface wing-tip endplates
upon the dihedral parameter $C_{l_{\psi}}$ of a $\frac{1}{5}$-scale model
of the type GB-5 controllable glide bomb. $\alpha = 6^{\circ}$;
$\delta_e = \delta_r = \delta_a = \delta_f = 0^{\circ}$.

Figure 10.- Effect of upper-surface endplates upon the
rolling-moment characteristics of a $\frac{1}{5}$-scale model of
the type GB-5 controllable glide bomb. $\alpha = 6^{\circ}$;
$\delta_e = \delta_r = \delta_f = \delta_a = 0^{\circ}$.

Figure 11.- Effect of vertical tail area removed equally from the twin vertical tails of a $\frac{1}{5}$-scale model of the type GB-5 controllable glide bomb. $\delta_e = \delta_a = \delta_f = 0^0$; $\alpha = 8^0$.

Figure 12.- Effect of removing vertical tail area from one of two vertical tails of a $\frac{1}{5}$-scale model of the type GB-5 controllable glide bomb. $\alpha = 8^0$; $\delta_e = \delta_r = \delta_a = \delta_f = 0^0$; right vertical tail off.

Figure 13.- The influence of vertical tail location upon the yawing-moment characteristics of a $\frac{1}{5}$-scale model of the type GB-5 controllable glide bomb in yaw. $\delta_e = \delta_a = \delta_r = \delta_f = 0^0$.

Figure 14.- Effect of reducing vertical tail size of a $\frac{1}{5}$-scale model of the type GB-5 controllable glide bomb. $\alpha = 8^0$; $\delta_e = \delta_r = \delta_a = \delta_f = 0^0$.

Figure 15.- Static lateral-stability characteristics of a $\frac{1}{5}$-scale model of the type GB-5 controllable glide bomb equipped with lower-surface, wing-tip, endplates 6 and vertical tail design 11. $\alpha = 6^0$; $\delta_e = \delta_r = \delta_a = \delta_f = 0^0$.

Figure 16.- Effect of angle of attack on the lateral stability characteristics of a $\frac{1}{5}$-scale model of the type GB-5 controllable glide bomb equipped with lower-surface, wing-tip endplates 6 and vertical tail design 11. $\delta_e = \delta_r = \delta_a = \delta_f = 0^0$.

Figure 17.- Effect of angle of attack on the rolling and yawing moment characteristics in yaw of a $\frac{1}{5}$-scale model of the type GB-5 controllable glide bomb. Vertical tail 1; $\delta_e = \delta_r = \delta_a = \delta_f = 0$.

Figure 18.- Variation of directional stability with angle of attack of a $\frac{1}{5}$-scale model of the type GB-5 controllable glide bomb as compared to that of an isolated rectangular wing.

FIGURE LEGENDS - Continued

Figure 19.- Effect of angle of attack on lateral-stability characteristics of a $\frac{1}{5}$-scale model of the type GB-5 controllable glide bomb equipped with original vertical tails 1 and forward tails 12. $\delta_r = \delta_f = \delta_e = \delta_a = 0^o$.

Figure 20.- Effect of angle of attack upon the directional stability parameter C_{n_ψ} of a $\frac{1}{5}$-scale model of the type GB-5 controllable glide bomb.

Figure 21.- Aileron characteristics of a $\frac{1}{5}$-scale model of the type GB-5 controllable glide bomb. $\psi = 0^o$; $\delta_e = \delta_r = \delta_f = 0^o$; $\delta_{a_L} = 0^o$.

Figure 22.- Effect of elevator deflection on the aerodynamic characteristics of a $\frac{1}{5}$-scale model of the type GB-5 controllable glide bomb. $\delta_r = \delta_a = \delta_f = 0^o$; $\psi = 0^o$.

Figure 23.- Effect of spoilers on the aerodynamic characteristics of a $\frac{1}{5}$-scale model of the type GB-5 controllable glide bomb. $\delta_a = \delta_r = \delta_f = 0^o$.

Figure 24.- Effect of double-split rudders on the aerodynamics characteristics of a $\frac{1}{5}$-scale model of the type GB-5 controllable glide bomb. Double-split rudders A; endplate 4; $\delta_a = \delta_r = \delta_e = 0^o$.

Figure 25.- Effect of double-split rudder deflections on the aerodynamic characteristics of a $\frac{1}{5}$-scale model of the type GB-5 controllable glide bomb. Double-split rudders A; $\delta_a = \delta_f = 0^o$; $\alpha = 8^o$; endplate 4.

Figure 26.- Effect of double-split rudders B upon the aerodynamic characteristics of a $\frac{1}{5}$-scale model of the type GB-5 controllable glide bomb. $\delta_e = \delta_a = \delta_f = 0^o$; endplate 3.

Figure 27.- Effect of double-split rudder deflection on the aerodynamic characteristics of a $\frac{1}{5}$-scale model of the type GB-5 controllable glide bomb; double-split rudders B; endplate 3; $\delta_a = \delta_f = 0^o$; $\alpha = 8^o$.

Figure 28.- Effect of outboard double-split flaps A upon the aerodynamic characteristics of a $\frac{1}{5}$-scale model of the type GB-5 controllable glide bomb $b_f = .42b$; $c_f = .30c$; $\delta_e = \delta_a = \delta_r = 0^o$.

Figure 29.- Effect of double-split flap deflections on the aerodynamic characteristics of a $\frac{1}{5}$-scale model of the type GB-5 controllable glide bomb. Outboard double-split flap A; $b_f = .42b$; $c_f = .30c$; $\delta_a = \delta_r = 0^o$; $\alpha = 8^o$.

Figure 30.- Effect of lower-surface inboard flaps 1 upon the aerodynamic characteristics of a $\frac{1}{5}$-scale model of the type GB-5 controllable glide bomb. $b_f = .42b$; $c_f = .30c$; $\delta_e = \delta_a = \delta_r = 0^o$.

Figure 31.- Effect of flap deflection on aerodynamic characteristics of a $\frac{1}{5}$-scale model of the type GB-5 controllable glide bomb. Lower surface, mid panel, split flap 1; $b_f = .42b$; $c_f = .30c$; $\alpha = 8^o$; $\delta_a = \delta_r = 0^o$.

Figure 32.- Effect of upper-surface inboard flaps 2 upon the aerodynamic characteristics of a $\frac{1}{5}$-scale model of the type GB-5 controllable glide bomb. $b_f = .42b$; $c_f = .30c$; $\delta_e = \delta_a = \delta_r = 0^o$.

Figure 33.- Effect of flap deflection on the aerodynamic characteristics of a $\frac{1}{5}$-scale model of the type GB-5 controllable glide bomb. Upper surface, inboard split flap 2; $b_f = .42b$; $c_f = .30c$; $\delta_a = \delta_r = 0^o$; $\alpha = 8^o$.

Figure 34.- Effect of upper-surface inboard flaps 3 upon the aerodynamic characteristics of a $\frac{1}{5}$-scale model of the type GB-5 controllable glide bomb. $b_f = .60b$; $c_f = .30c$; $\delta_e = \delta_a = \delta_r = 0^o$.

Figure 35.- Effect of flap deflection on the aerodynamic characteristics of a $\frac{1}{5}$-scale model of the type GB-5 controllable glide bomb. Upper surface, inboard split flap 3; $b_f = .60b$; $c_f = .30c$; $\delta_a = \delta_r = 0$; $\alpha = 8^o$.

FIGURE LEGENDS - Concluded

Figure 36.- Effect of upper-surface, outboard flaps 4 upon the aerodynamic characteristics of a $\frac{1}{5}$-scale model of the type GB-5 controllable glide bomb. $b_f = .60b$; $c_f = .30c$; $\delta_e = \delta_a = \delta_r = 0^\circ$.

Figure 37.- Effect of flap deflection on the aerodynamic characteristics of a $\frac{1}{5}$-scale model of the type GB-5 controllable glide bomb. Upper-surface, outboard split flap 4; $b_f = .60b$; $c_f = .30c$; $\delta_a = \delta_r = 0$; $\alpha = 8^\circ$.

Figure 38.- Effect of upper-surface flaps 5 upon the aerodynamic characteristics of a $\frac{1}{5}$-scale model of the type GB-5 controllable glide bomb. $b_f = .60b$; $c_f = .30c$; $\delta_e = \delta_a = \delta_r = 0^\circ$.

Figure 39.- Effect of flap deflection on the aerodynamic characteristics of a $\frac{1}{5}$-scale model of the type GB-5 controllable glide bomb. Upper surface mid-panel split flap 5; $b_f = .60b$; $c_f = .30c$; $\delta_a = \delta_r = 0$; $\alpha = 8^\circ$.
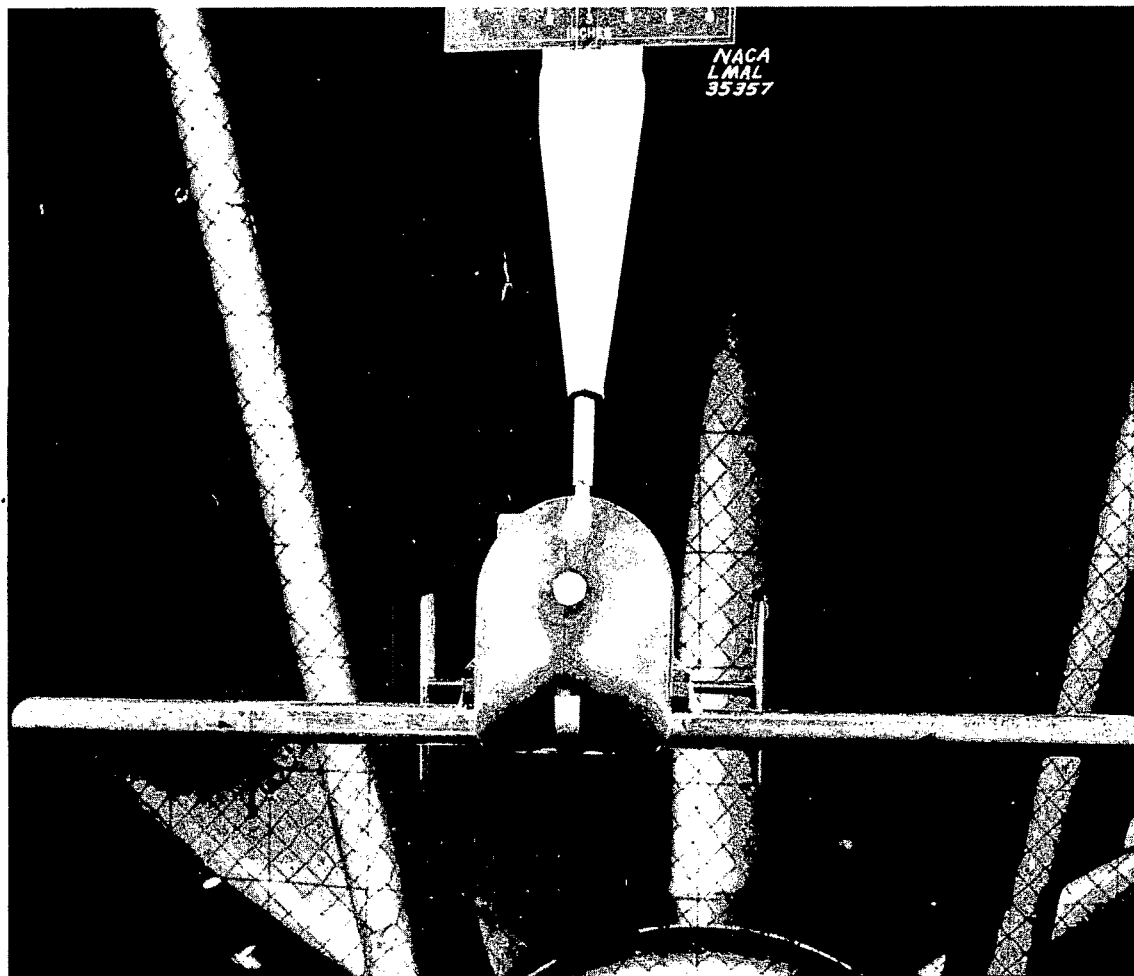
Figure 1.- Photograph of a $\frac{1}{5}$-scale model of the type
GB-5 controllable glide bomb mounted inverted on the
free-flight tunnel balance strut.

Figure 2.- Three view sketch of the type GB-5 controllable glide bomb as originally received. All dimensions are in inches.

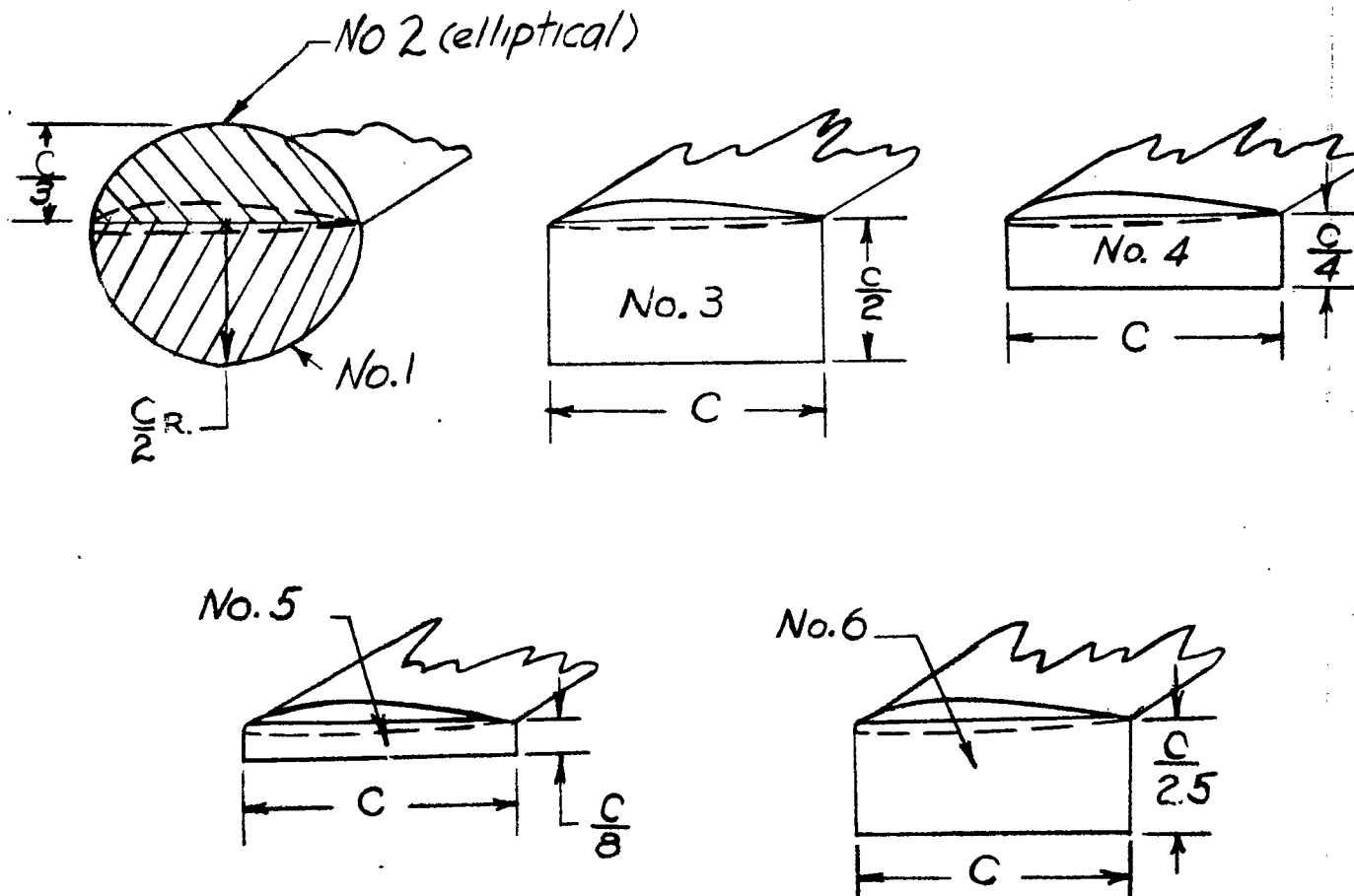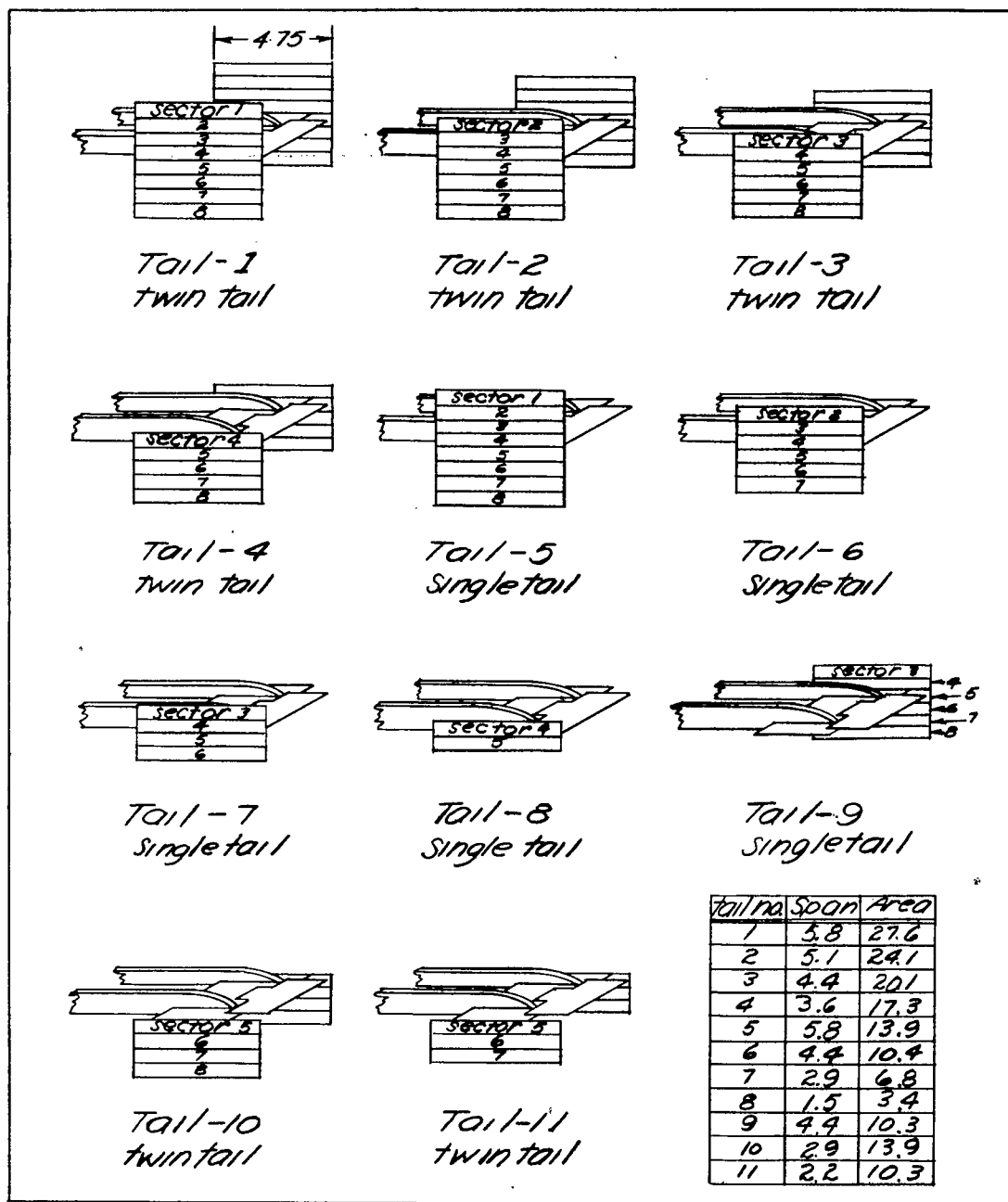Figure 3.- Photographs of $\frac{1}{5}$-scale model of type GB-5 controllable glide bomb.
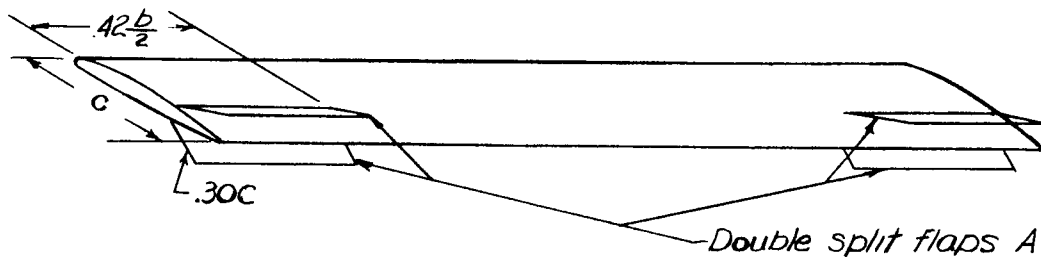
Figure 4.- Sketches of vertical wing-tip end plates tested in the free-flight-tunnel investigation of a $\frac{1}{5}$-scale model of the type GB-5 controllable glide bomb.

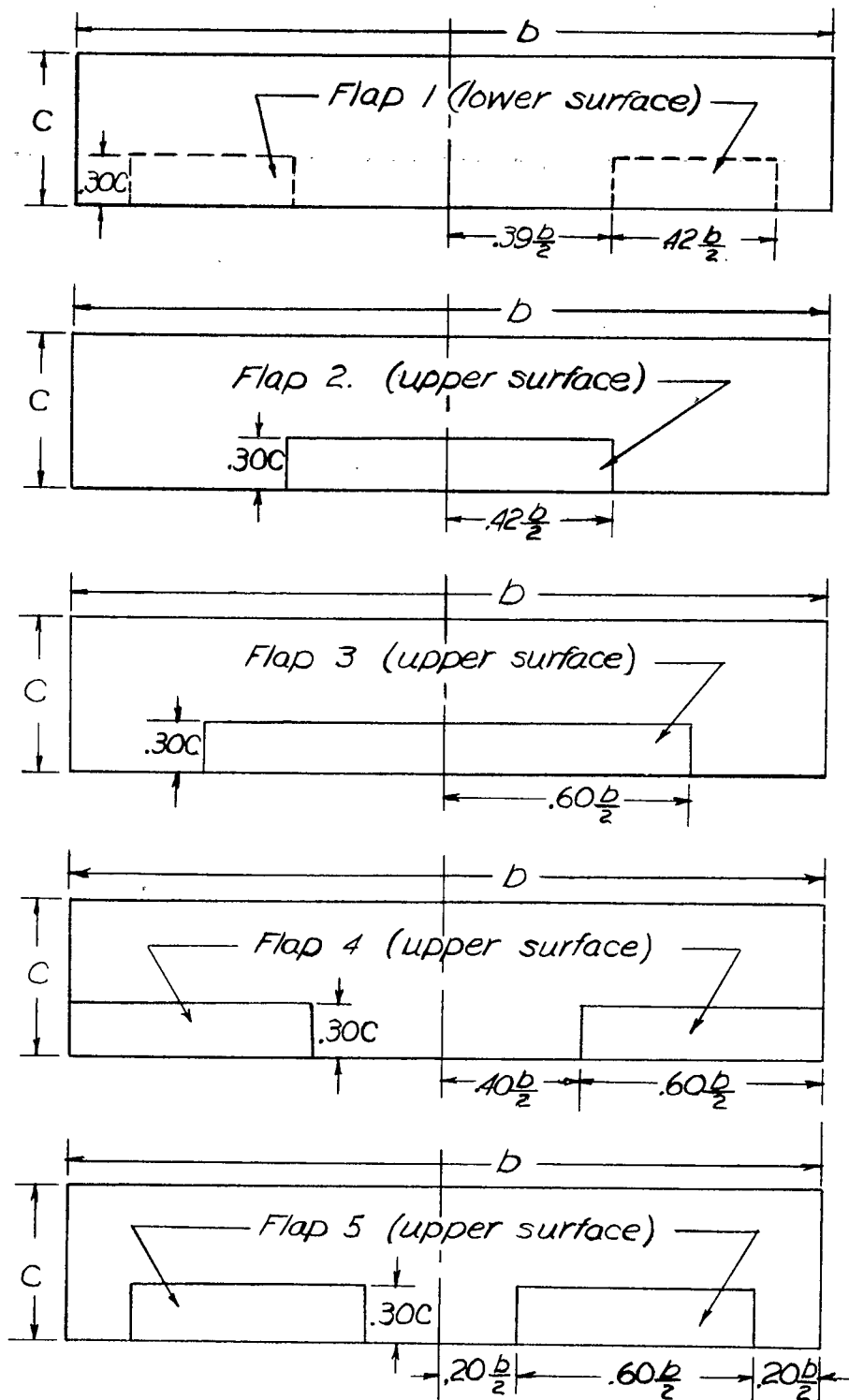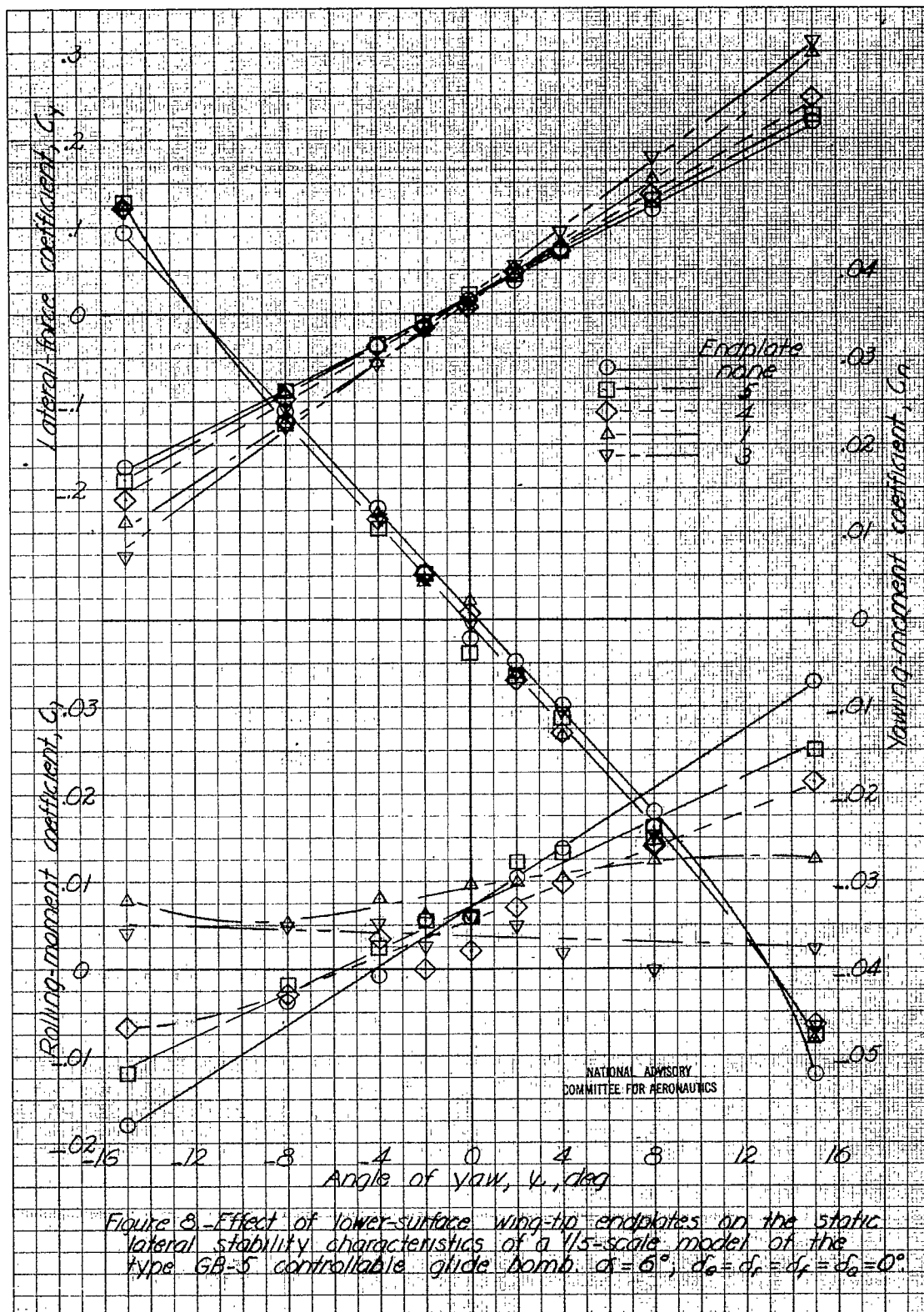| tail no.	Span	Area
1	5.8	27.6
2	5.1	24.1
3	4.4	20.1
4	3.6	17.3
5	5.8	13.9
6	4.4	10.4
7	2.9	6.8
8	1.5	3.4
9	4.4	10.3
10	2.9	13.9
11	2.2	10.3
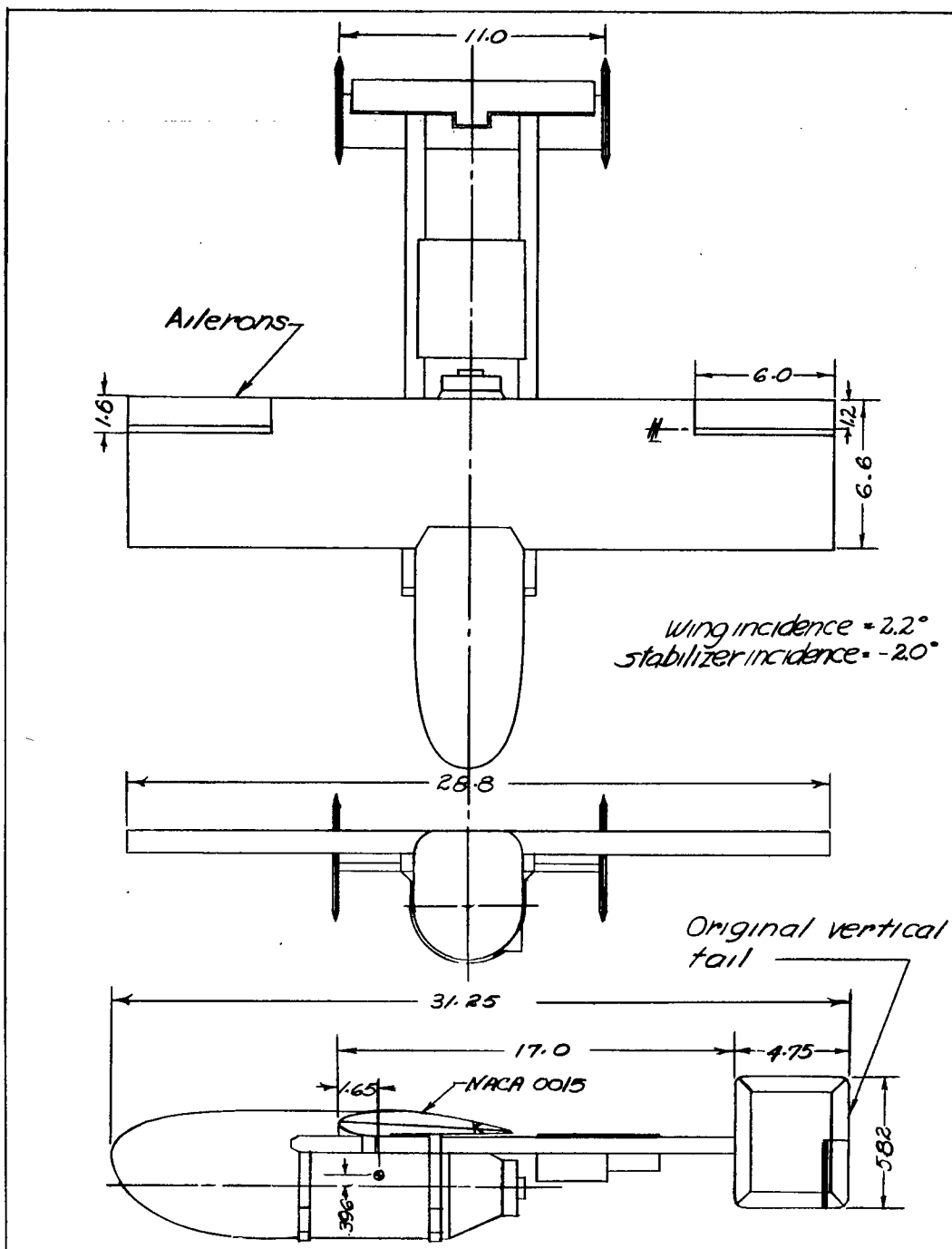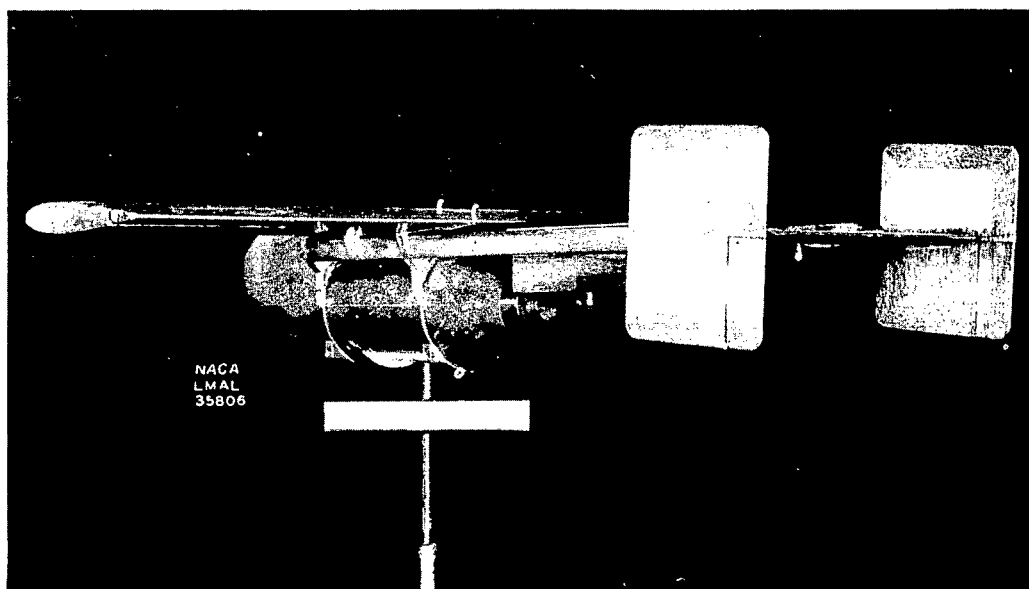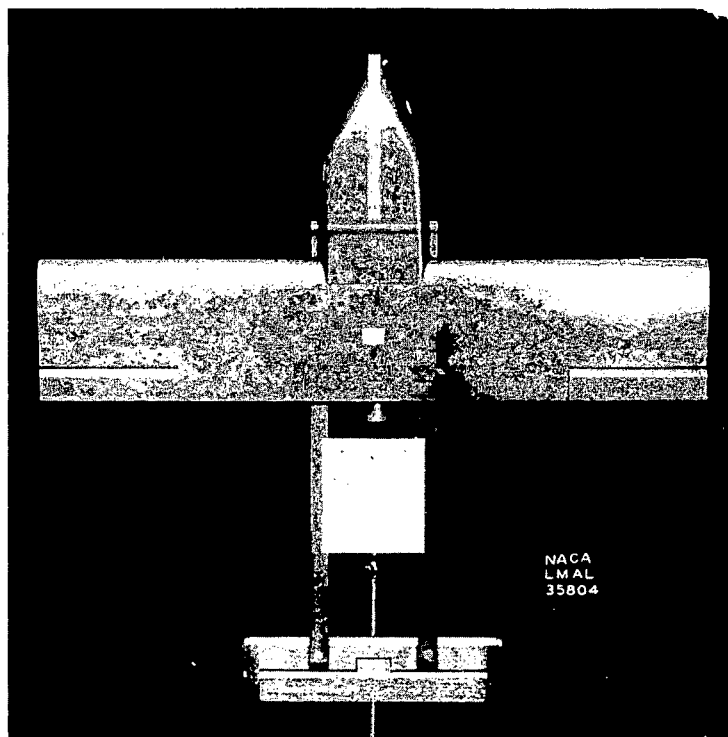
Note - Chords of all tails equal to chord of tail-1. Sectors indicate manner of subdivision of tail-1 by eighths to form other designs.

Figure 5.- Sketches of aft vertical tail surfaces installed on a $\frac{1}{5}$-scale model of the type GB-5 controllable glide bomb tested in the free-flight tunnel.

Figure 6.- Sketch of forward fins and ailerons tested on a $\frac{1}{5}$-scale model of the type GB-5 controllable glide bomb in the free-flight tunnel.

Spoilers 2 — ₵ wing

Spoiler 1.

.20 C

.06C

.39 $\frac{b}{2}$ — .61 $\frac{b}{2}$

b

C

End plate 3

End plate 4

$\frac{c}{2}$

$\frac{c}{4}$

C

C

Split rudders A

Split rudders B

.30C

.30 C
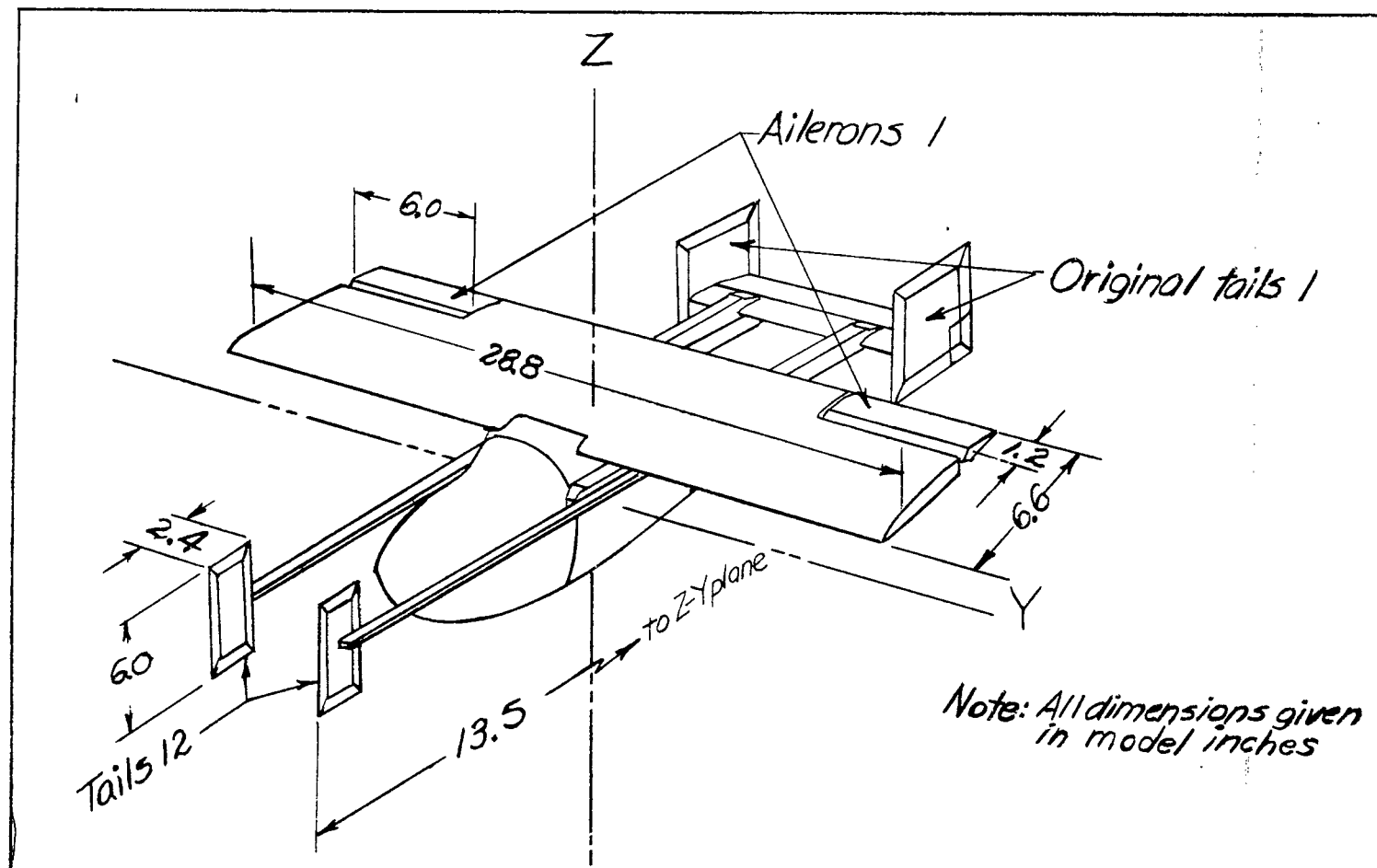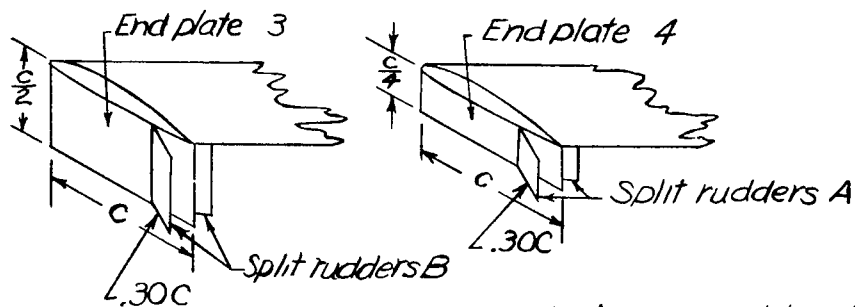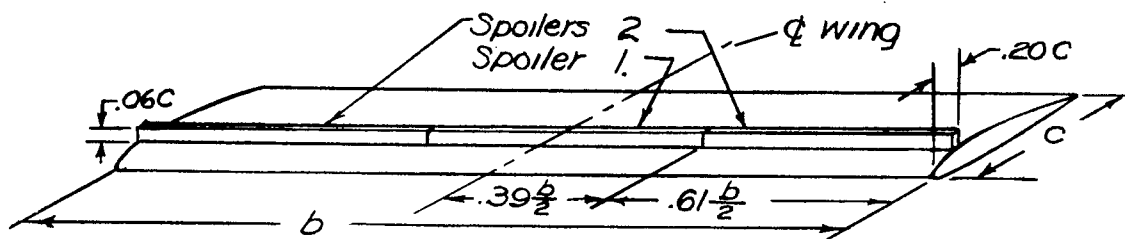
Note: b = 28.8 model inches
C = 6.6 model inches

.42 $\frac{b}{2}$

C

.30C

Double split flaps A

Figure 7.- Sketches of glide-path controls tested in the free-flight tunnel
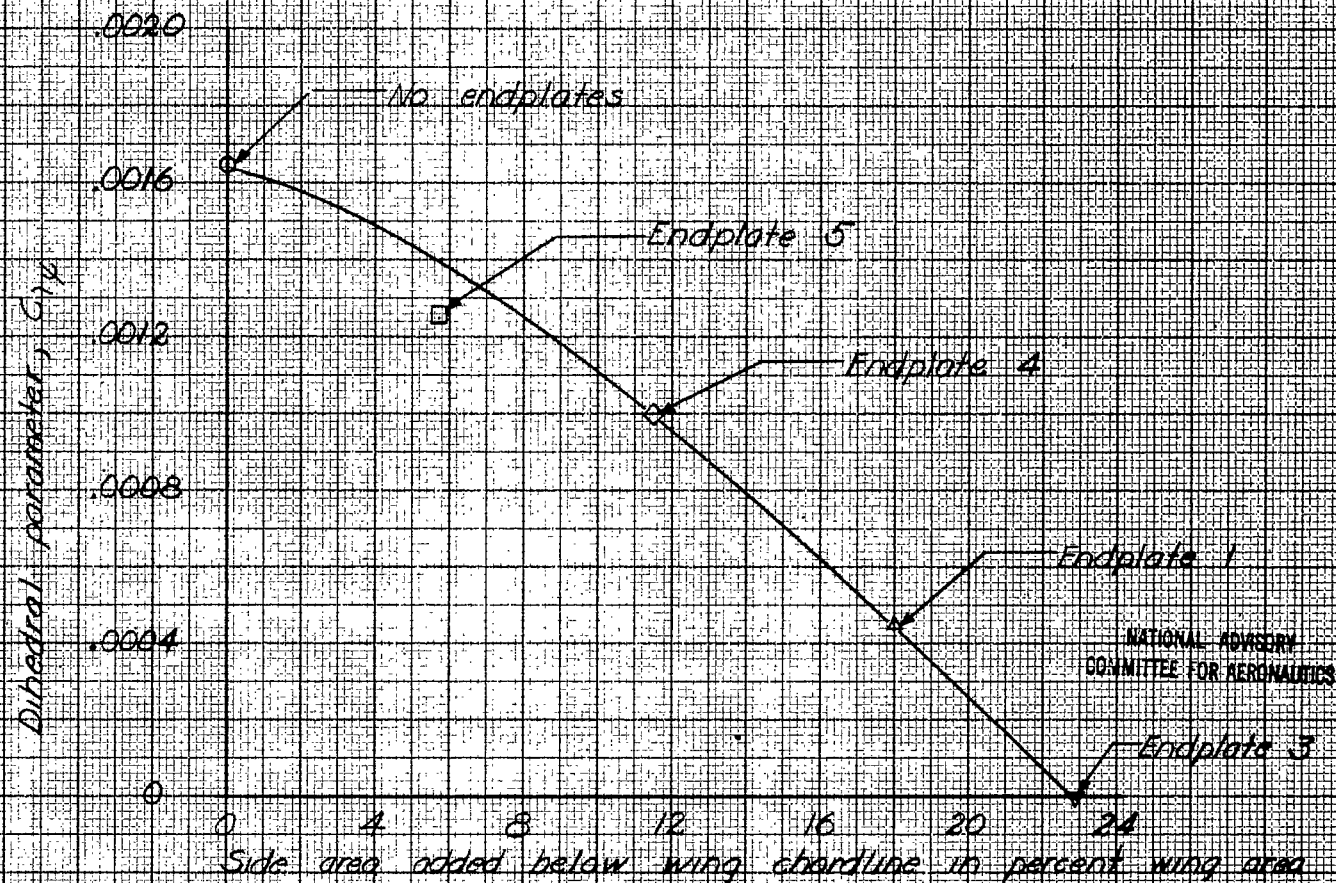investigation of a $\frac{1}{5}$ -scale model of the type GB-5 controllable glide bomb.
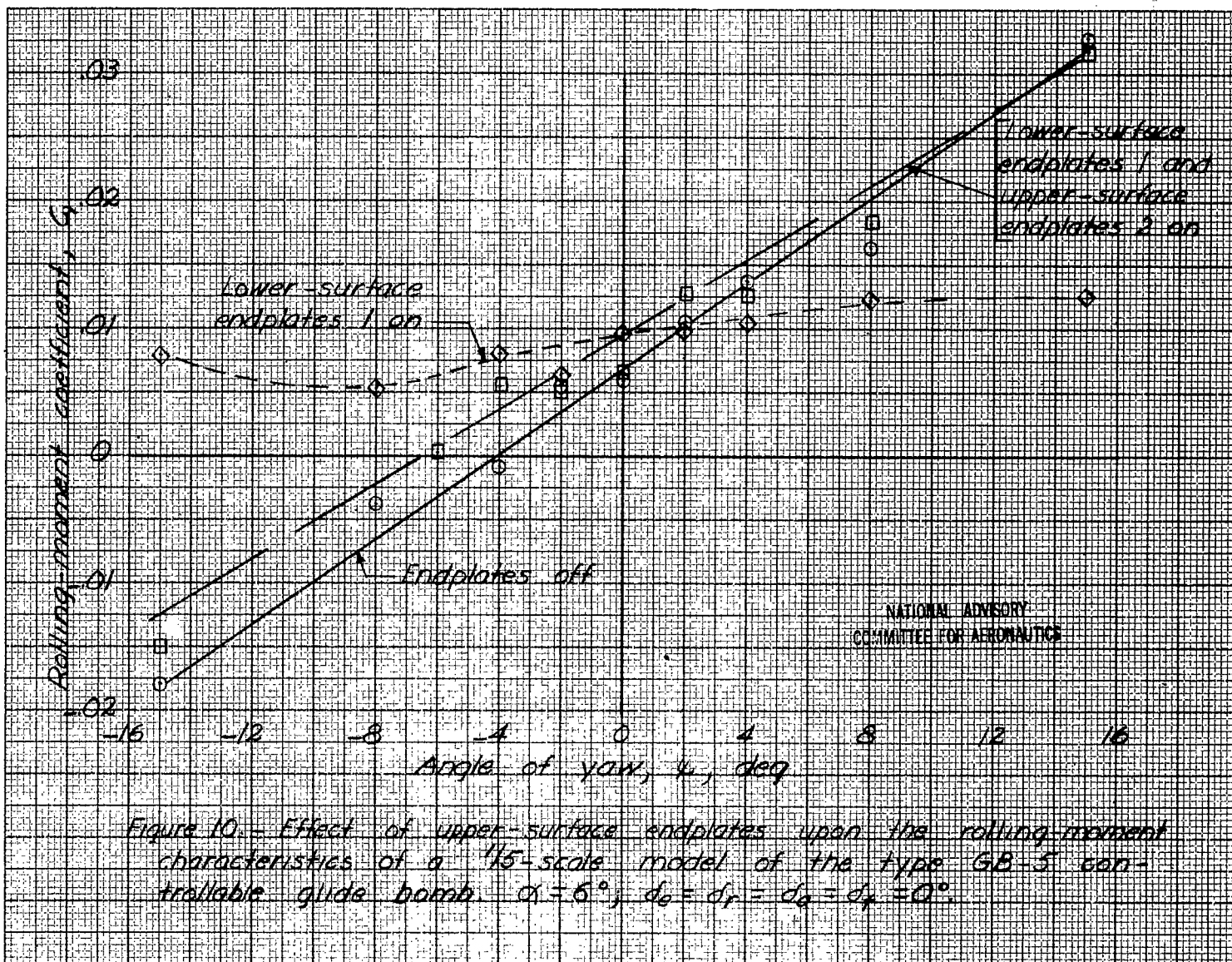
Figure 7.- Continued.

Figure 8.-Effect of lower-surface wing-tip endplates on the static lateral stability characteristics of a 1/5-scale model of the type GB-5 controllable glide bomb. $\alpha = 6°$, $d_e = d_r = d_f = d_a = 0°$.
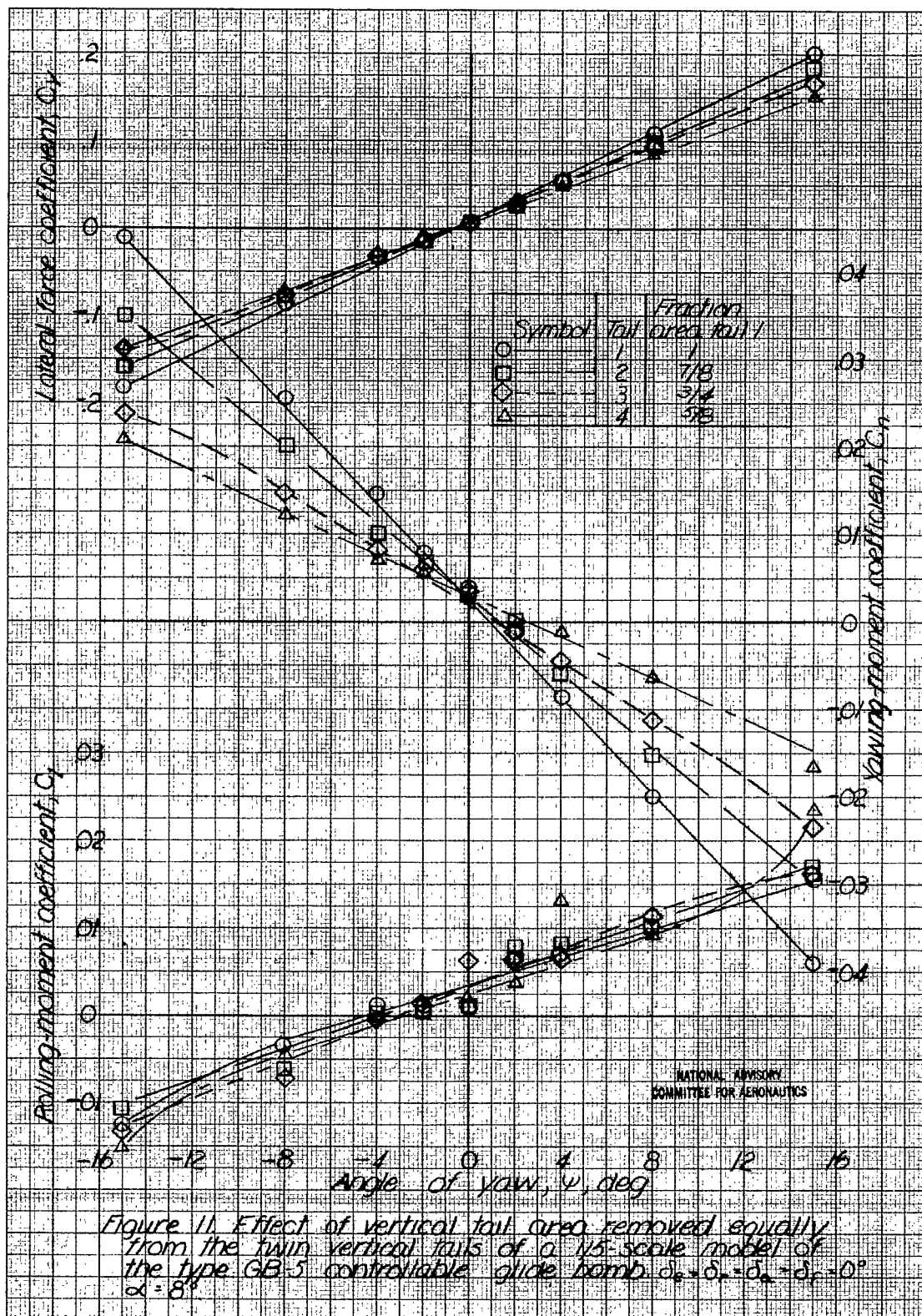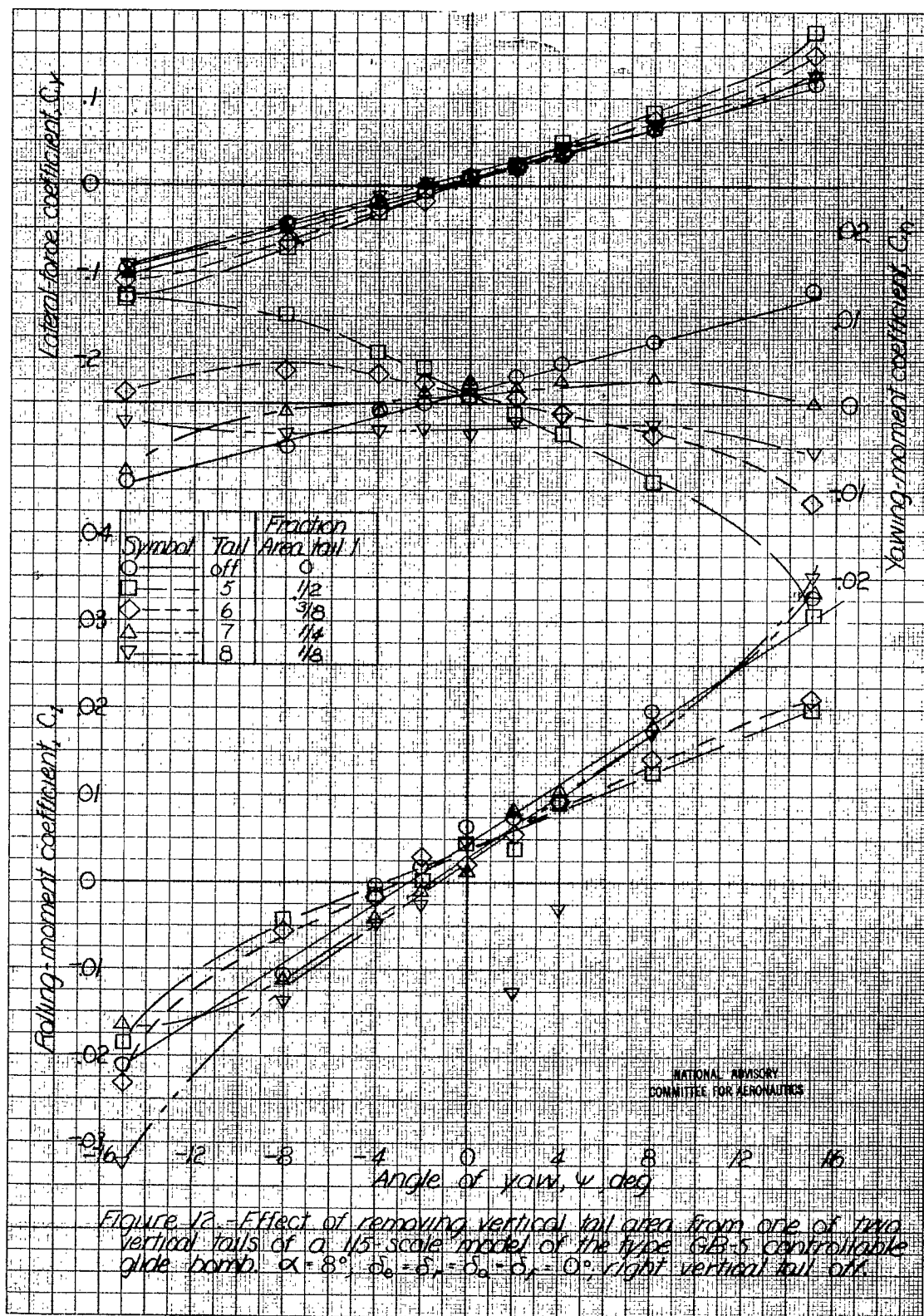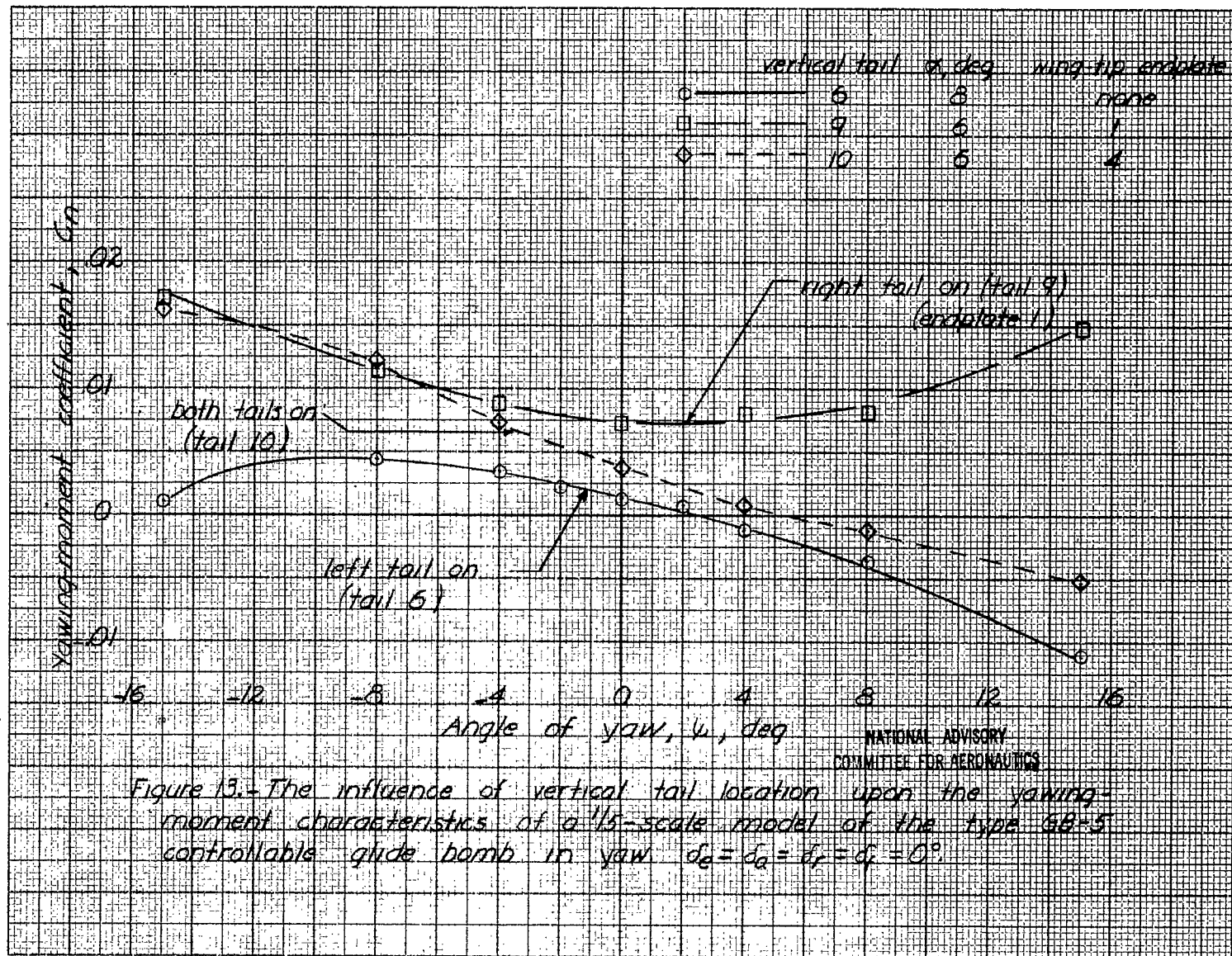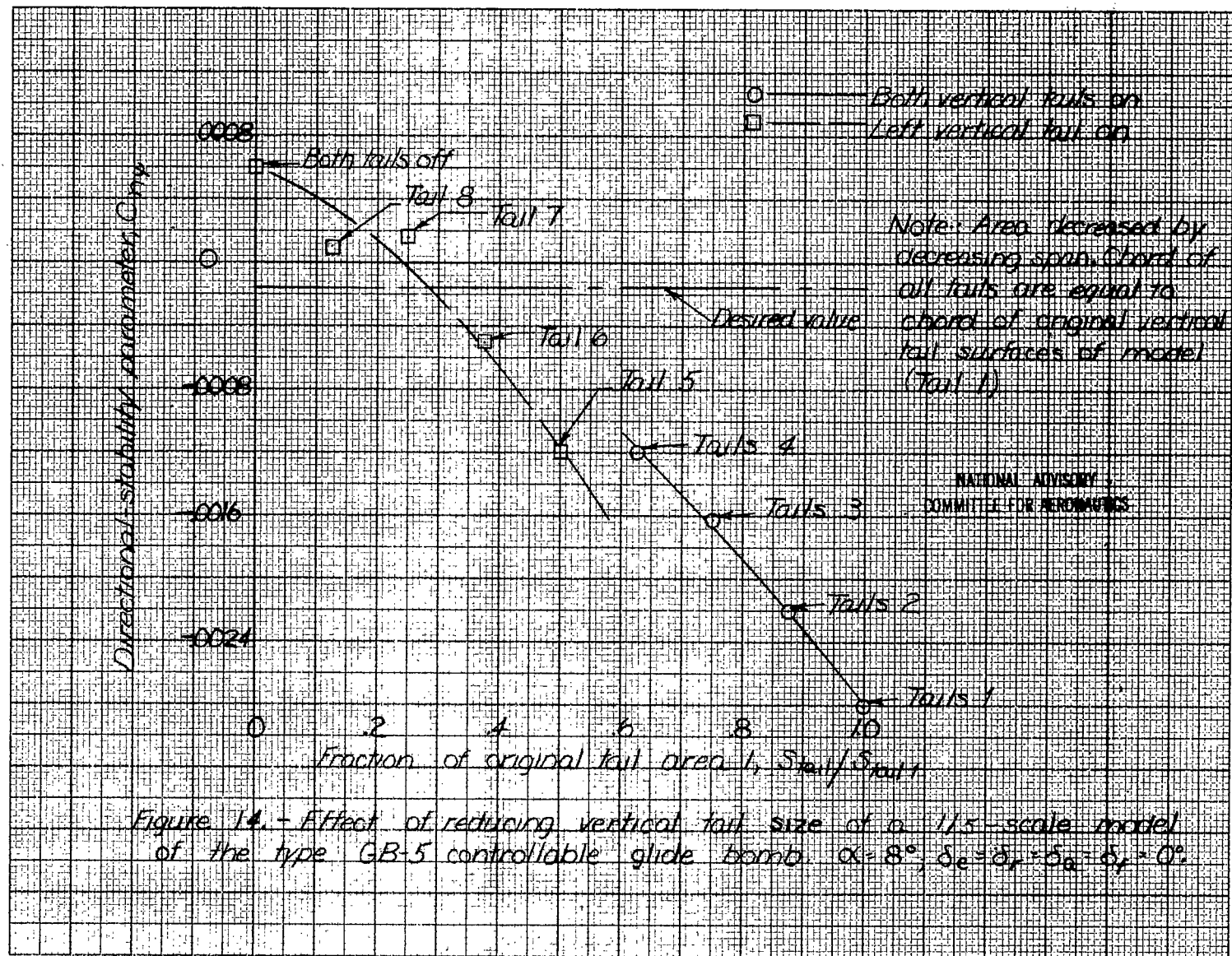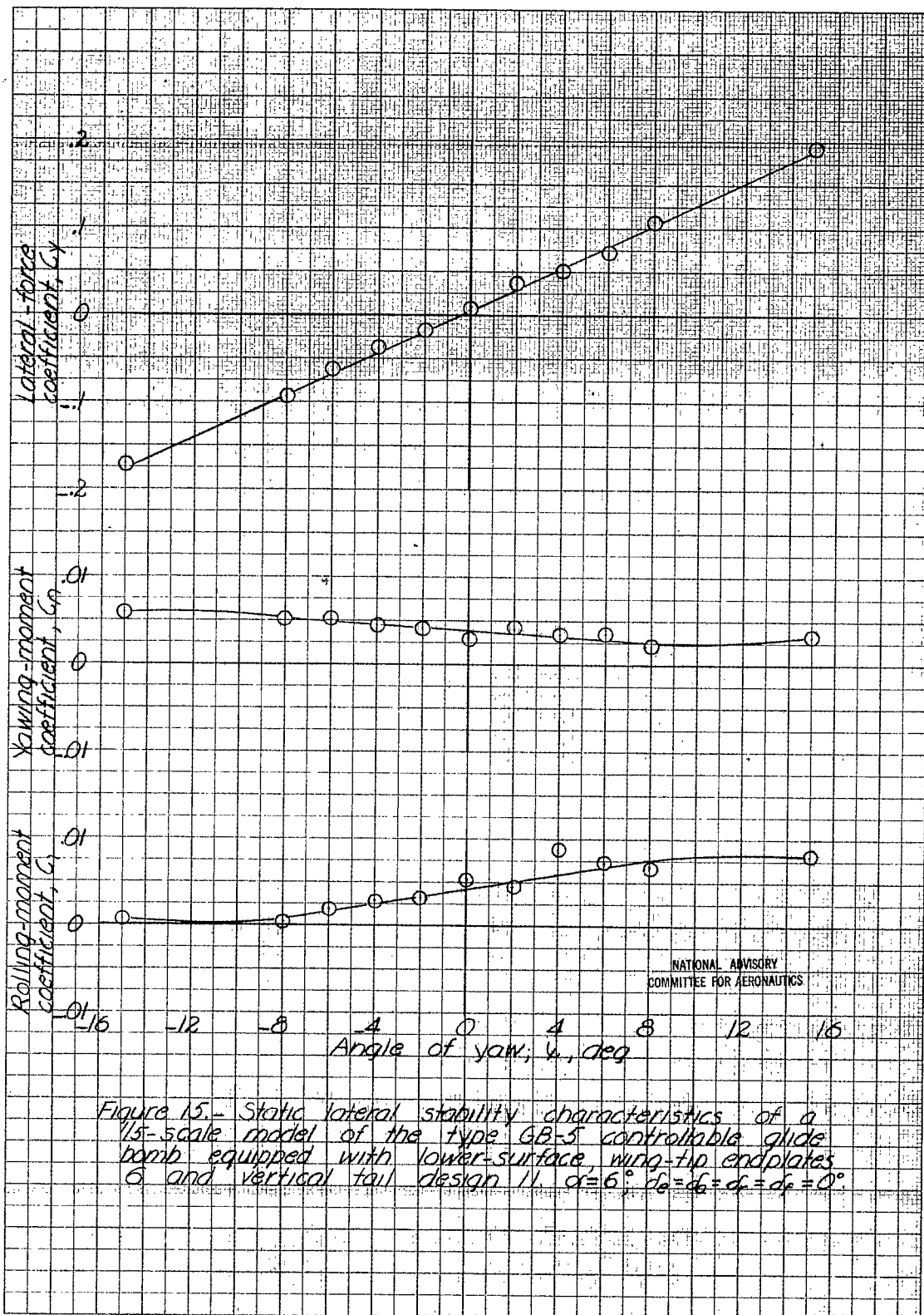
Figure 9 – Effect of lower-surface wing-tip endplates upon the dihedral parameter C_{l_ψ} of a 1/5-scale model of the type GB-5 controllable glide bomb. $\alpha = 6°$, $\delta_e = \delta_f = \delta_a = \delta_r = 0°$.

Figure 10.- Effect of upper-surface endplates upon the rolling-moment characteristics of a 1/5-scale model of the type GB-5 controllable glide bomb. $\alpha = 6°$; $\delta_e = \delta_r = \delta_a = \delta_f = 0°$.

Lateral-force coefficient C_Y
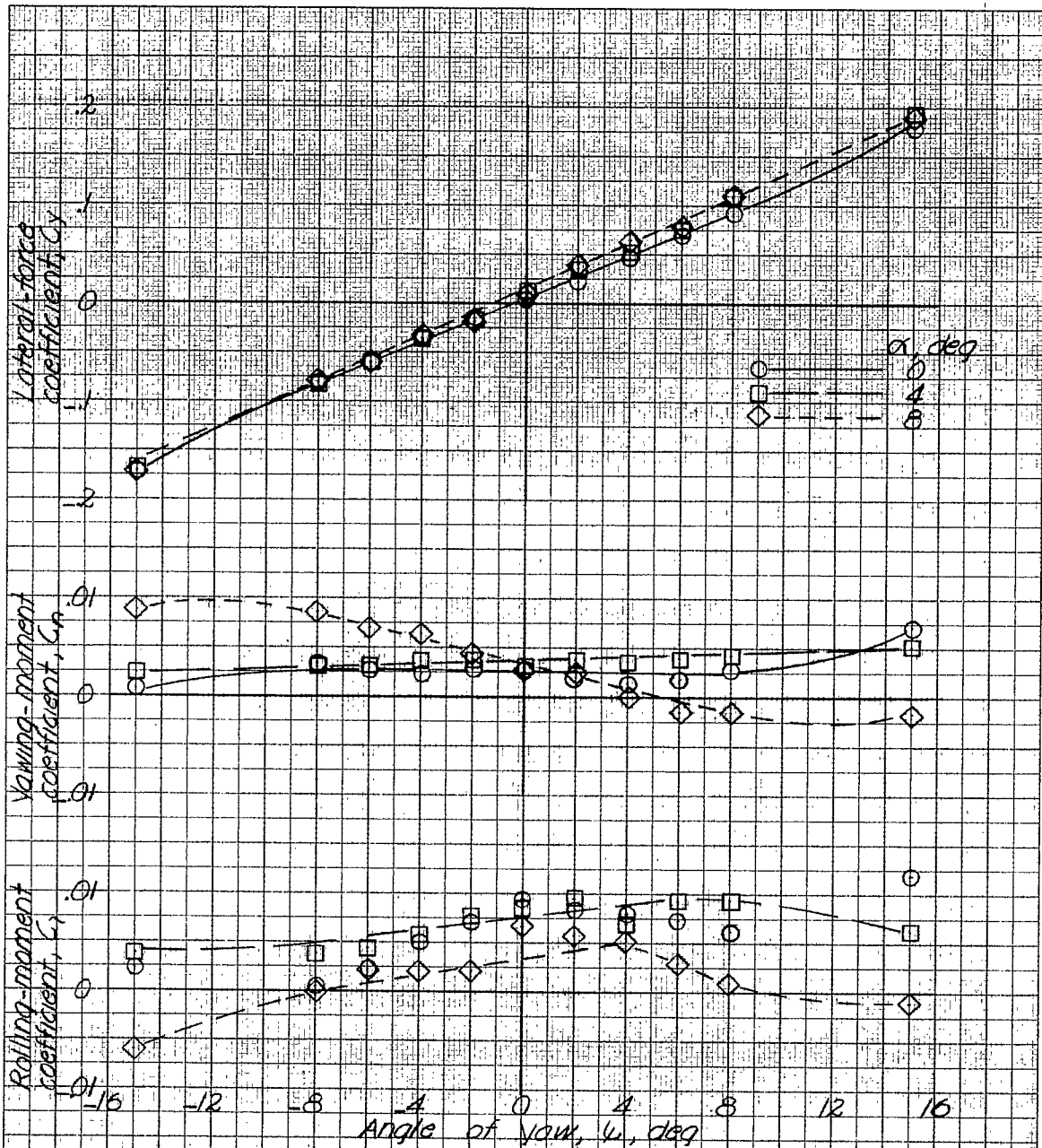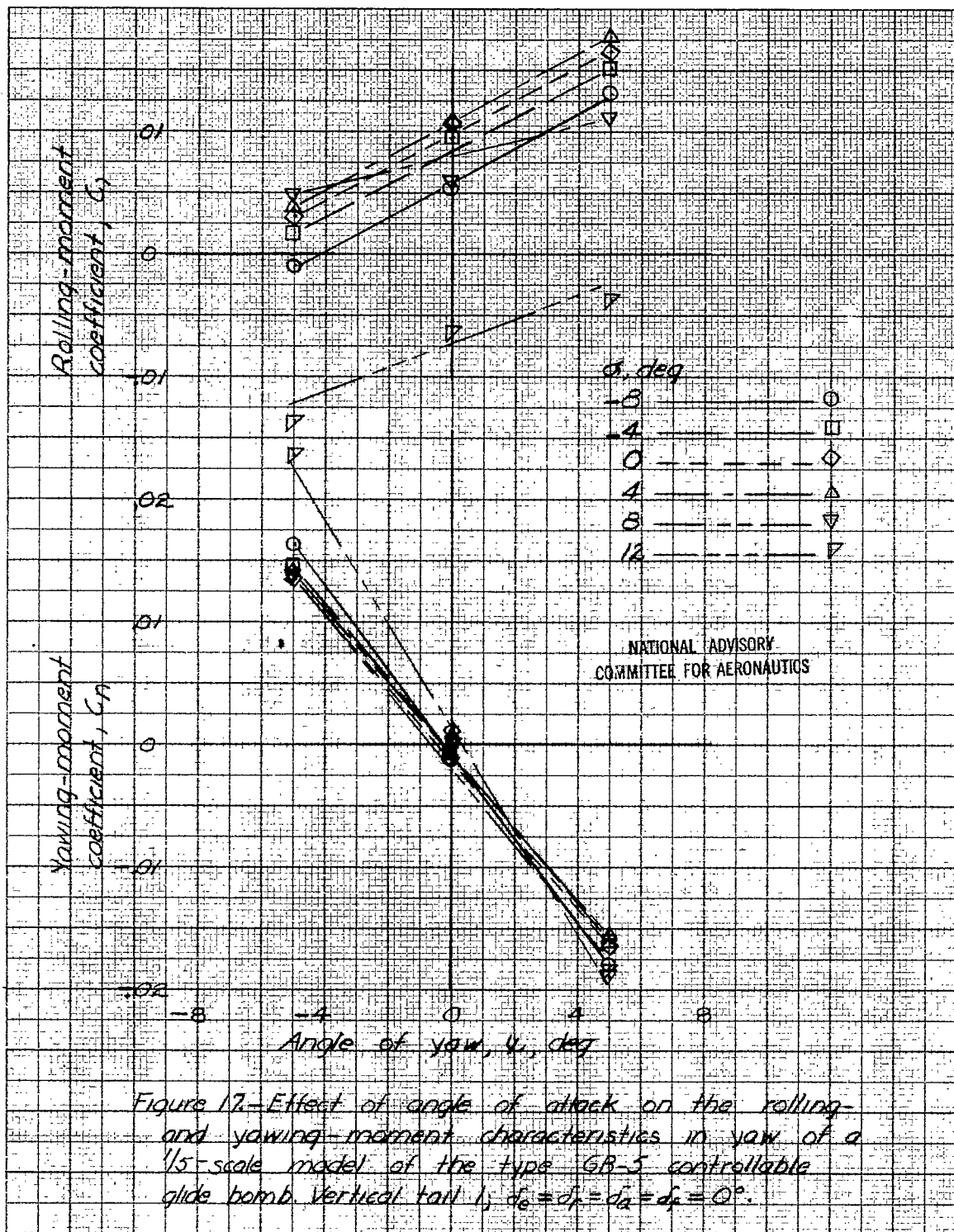
.2

.1

0

-.1

-.2

Rolling-moment coefficient C_l

.03

.02

.01

0

-.1

Yawing-moment coefficient C_n

.04

.03

.02

.01

0

-.01

-.02

-.03

-.04

Symbol	Tail	Fraction area tail 1
○	1	1
□	2	7/8
◇	3	3/4
△	4	5/8

-16   -12   -8   -4   0   4   8   12   16

Angle of yaw, ψ, deg

Figure 11. Effect of vertical tail area removed equally from the twin vertical tails of a 1/5-scale model of the type GB-5 controllable glide bomb. $\delta_a = \delta_e = \delta_r = \delta_f = 0°$; $\alpha = 8°$

Lateral-force coefficient, C_Y

.1

0

-.1

-.2

Yawing-moment coefficient, C_n

.02

.01

0

-.01

-.02

Rolling-moment coefficient, C_l

.04

.03

.02

.01

0

-.01

-.02

-.03

Symbol	Tail	Fraction Area tail 1
○	off	0
□	5	1/2
◇	6	3/8
△	7	1/4
▽	8	1/8

-16   -12   -8   -4   0   4   8   12   16

Angle of yaw, ψ, deg

Figure 12.- Effect of removing vertical tail area from one of two vertical tails of a 1/5-scale model of the type GB-5 controllable glide bomb. α = 8°, δ_a = δ_r = δ_e = δ_f = 0°, right vertical tail off.

Figure 13.- The influence of vertical tail location upon the yawing-moment characteristics of a 1/5-scale model of the type GB-5 controllable glide bomb in yaw. $\delta_e = \delta_a = \delta_r = \delta_f = 0°$.

Figure 14.- Effect of reducing vertical tail size of a 1/5-scale model of the type GB-5 controllable glide bomb. $\alpha = 8°$, $\delta_e = \delta_r = \delta_a = \delta_t = 0°$.

Figure 15.- Static lateral stability characteristics of a 15-scale model of the type GB-5 controllable glide bomb equipped with lower-surface wing-tip endplates 6 and vertical tail design 11. $\alpha = 6°$; $\delta_e = \delta_a = \delta_r = \delta_f = 0°$.
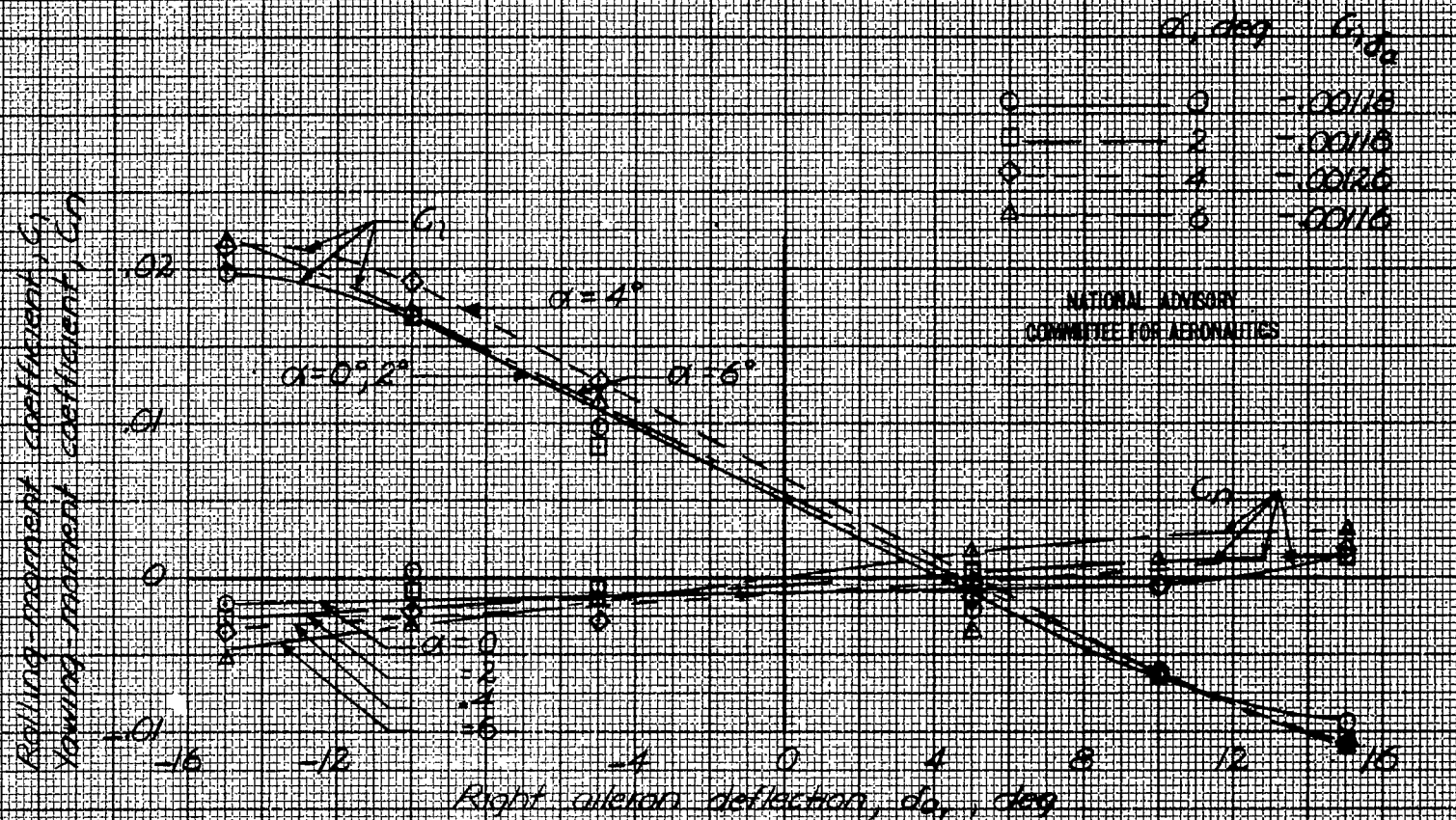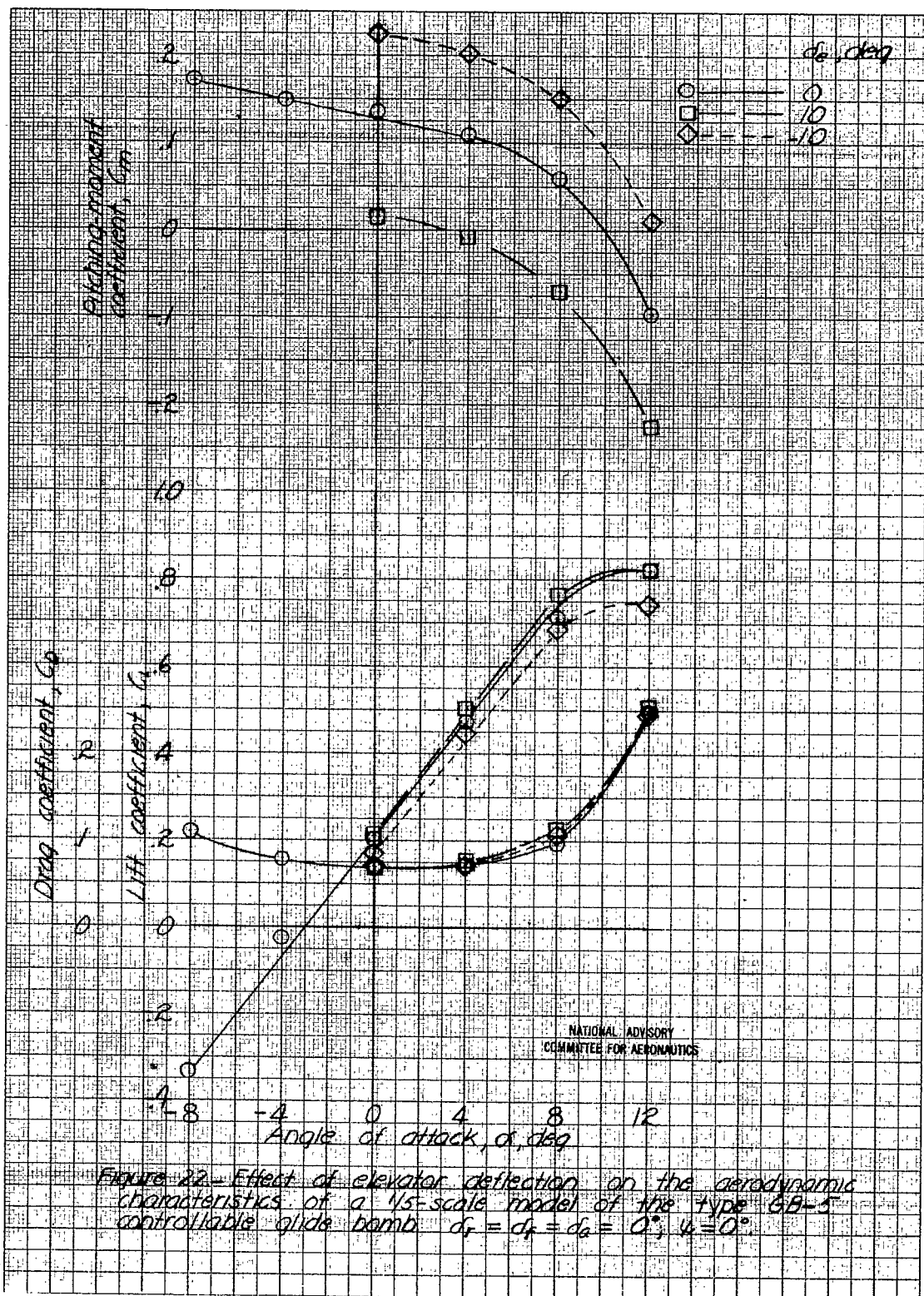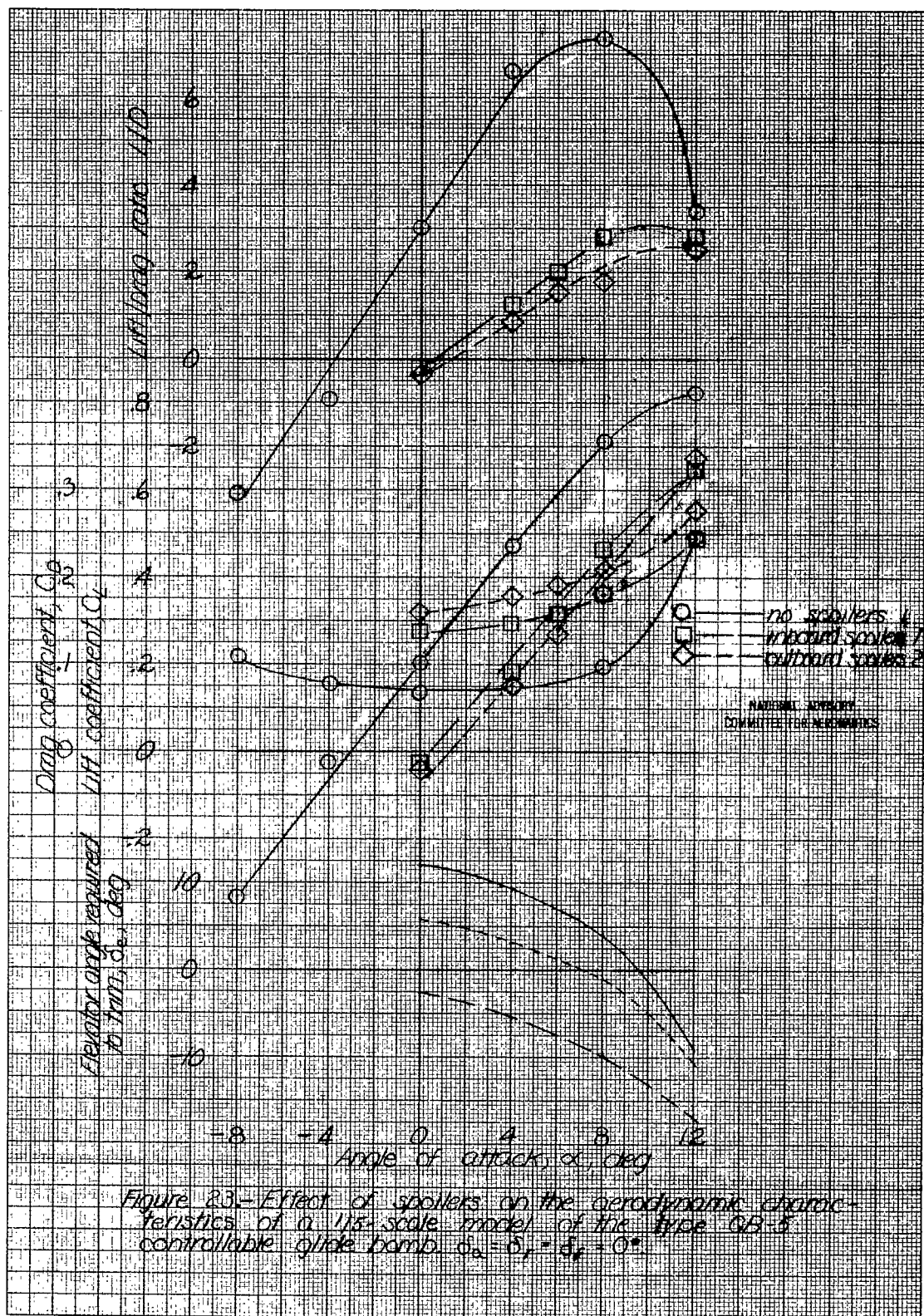
Figure 16.- Effect of angle of attack on the lateral stability characteristics of a 1/5-scale model of the type GB-5 controllable glide bomb equipped with lower-surface wing-tip endplates 6 and vertical tail design 11. $d_e = d_r = d_a = d_f = 0°$.

Figure 17.—Effect of angle of attack on the rolling- and yawing-moment characteristics in yaw of a 1/5-scale model of the type GB-5 controllable glide bomb. Vertical tail 1, $d_e = d_r = d_a = d_s = 0°$.

Figure 18.- Variation of directional stability with angle of attack of a
1/5-scale model of the type GB-5 controllable guide bomb as
compared to that of an isolated rectangular wing.

Figure 19.- Effect of angle of attack on lateral stability characteristics of a 1/5-scale model of the type GB-5 controllable glide bomb equipped with original vertical tails I and forward tails 12. $\delta_r = \delta_f = \delta_e = \delta_a = 0°$

Figure 20.- Effect of angle of attack upon the directional stability parameter $C_{n\psi}$ of a 1/5-scale model of the type GB-5 controllable glide bomb.

Figure 21.— Aileron characteristics of a 1/5 scale model of the type GB-3 controllable glide bomb. $\psi = 0°$; $\delta_e = \delta_f = \delta_g = 0°$; $\delta_{a_L} = 0°$.

Figure 22.- Effect of elevator deflection on the aerodynamic characteristics of a 1/5-scale model of the type GB-5 controllable glide bomb. $d_r = d_f = d_G = 0°$; $\psi = 0°$.

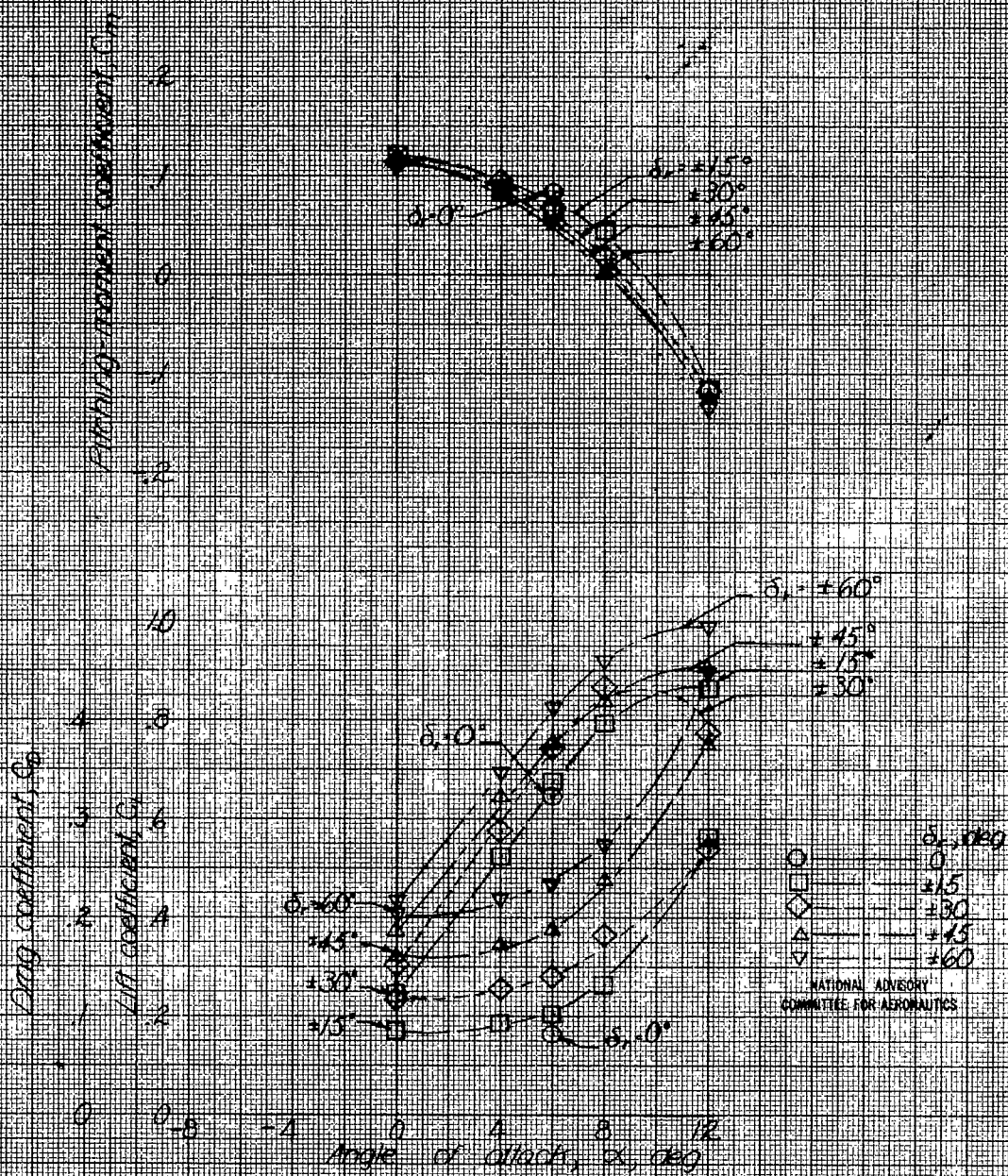Figure 23.- Effect of spoilers on the aerodynamic characteristics of a 1/5-scale model of the type GB-5 controllable glide bomb $\delta_a = \delta_f = \delta_t = 0°$.

Figure 24.— Effect of double-split rudders on the aerodynamic characteristics of a 1/5-scale model of the type GB-5 controllable glide bomb. Double-split rudders A; endplate 4; $\delta_a = \delta_f = \delta_e = 0°$.
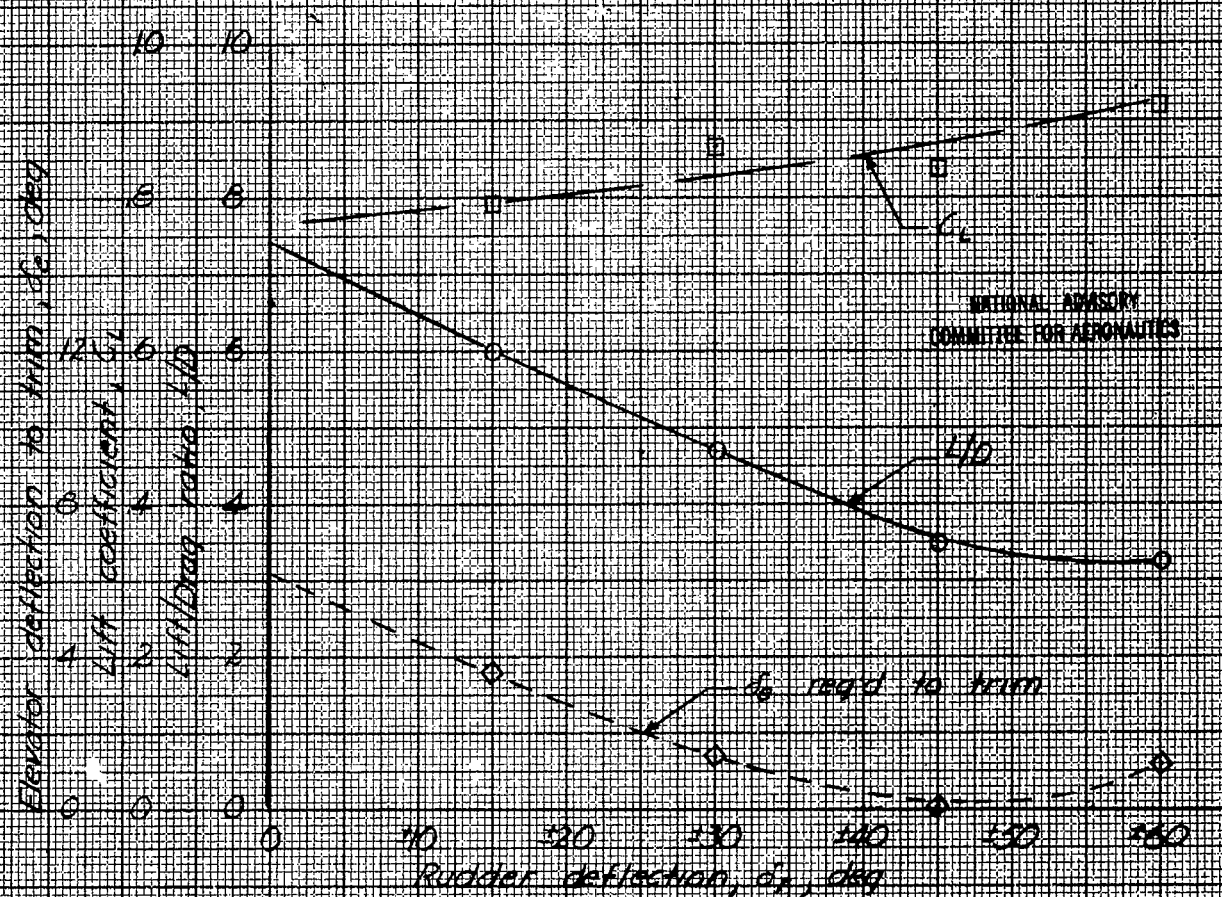
Figure 25.- Effect of double-split rudder deflection on the aerodynamic characteristics of a 1/5-scale model of the type GB-5 controllable glide bomb. Double-split rudders A; $\delta_a = \delta_r = 0°$; end plate 4; $\alpha = 8°$.
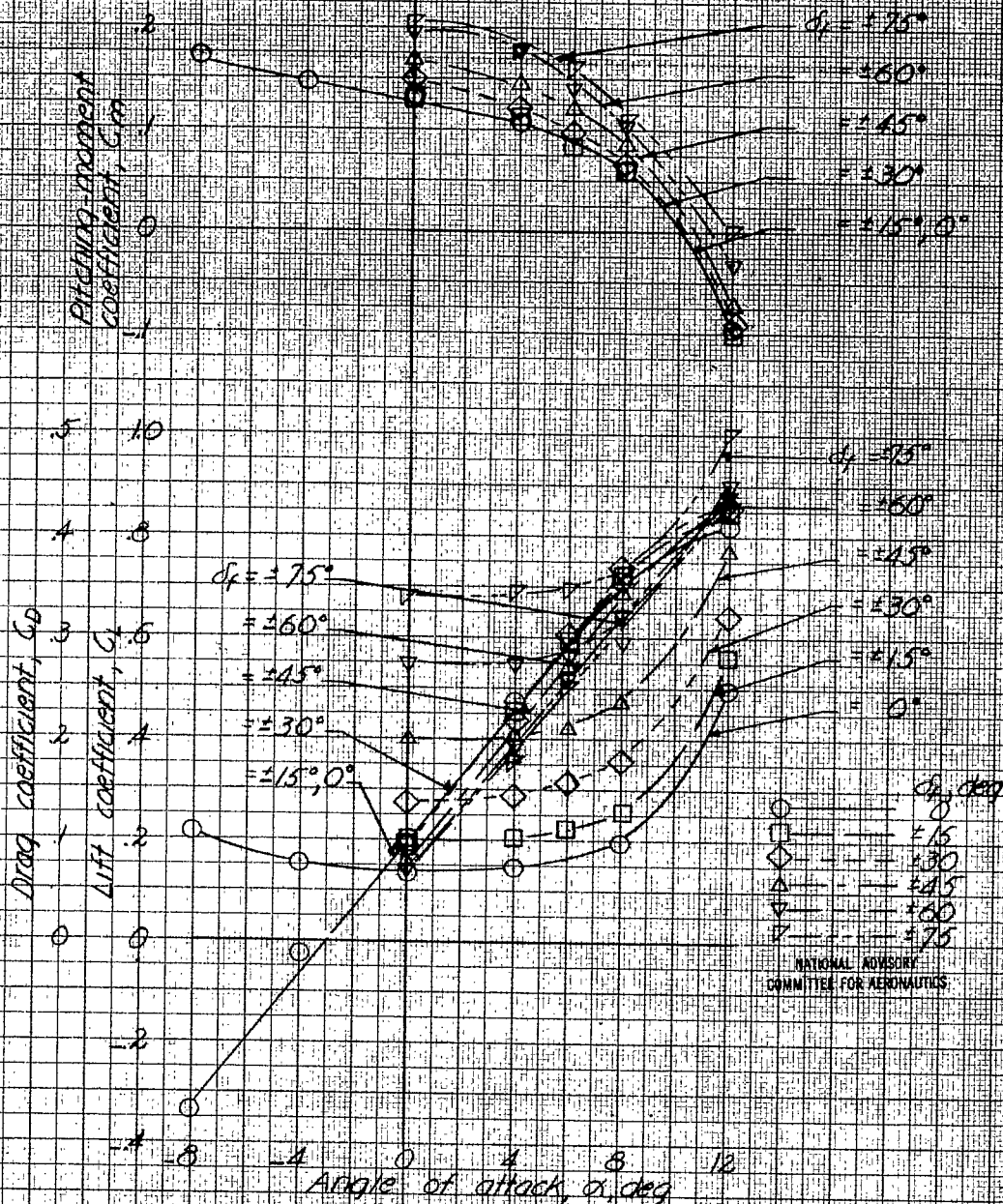
Figure 26.- Effect of double split rudders B upon the aerodynamic characteristics of a 1/5-scale model of the type GB-5 controllable glide bomb $\delta_a = \delta_e; \delta_f = 0^\circ$; endplate 3.

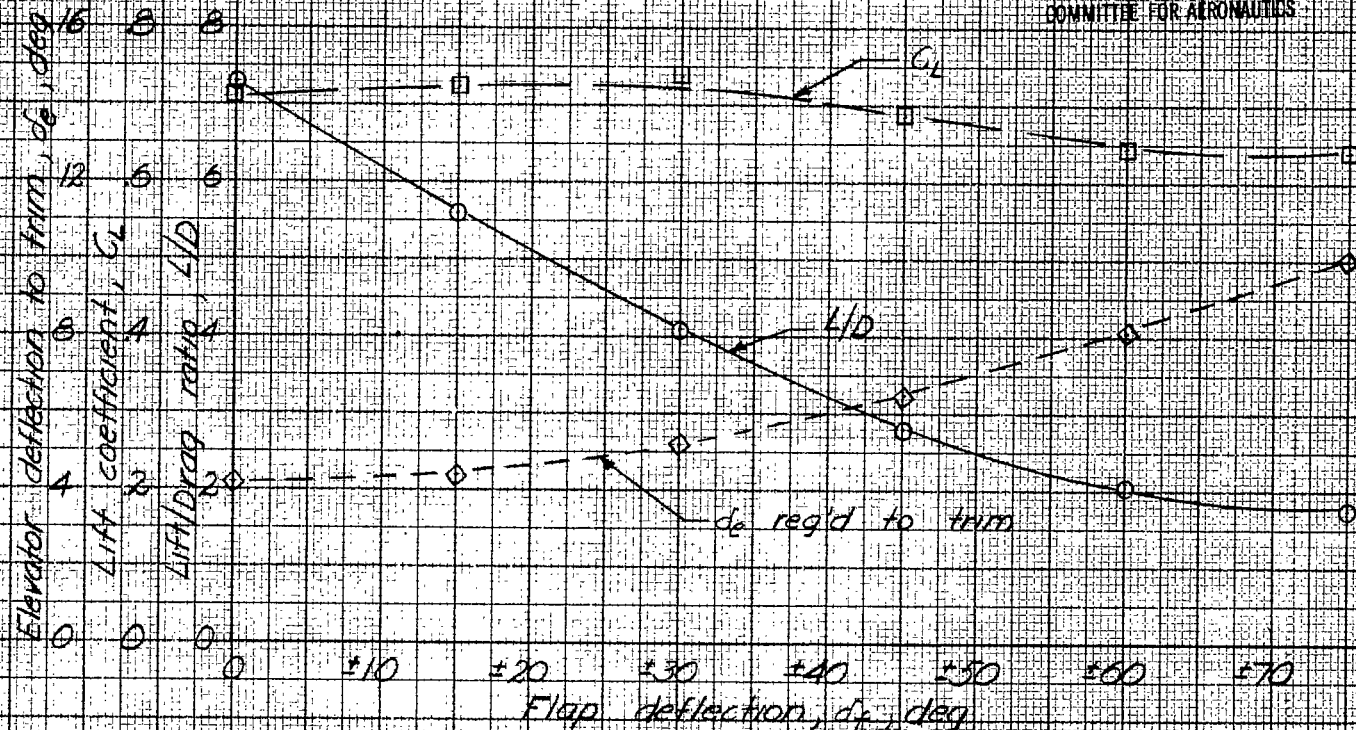Figure 27.-Effect of double split rudder deflection on the aerodynamic characteristics of a 1/5-scale model of the GB-5 controllable glide bomb. Double-split rudders δ_r; tailplate 3; $i_t = \delta_f = 0°$, $\alpha = 8°$.

Figure 28.- Effect of outboard double-split flaps A upon the aerodynamic characteristics of a 1/5-scale model of the type GB-5 controllable glide bomb. $b_f = 0.42b$; $c_f = 0.30c$; $d_e = d_a = d_r = 0°$.

Figure 29.- Effect of double-split flap deflections on the aerodynamic characteristics of a $\frac{1}{5}$-scale model of the type GB-5 controllable glide bomb. Outboard double-split flap A, $b_f = 0.42b$; $c_f = 0.30c$; $d_a = d_r = 0°$; $\alpha = 8°$.
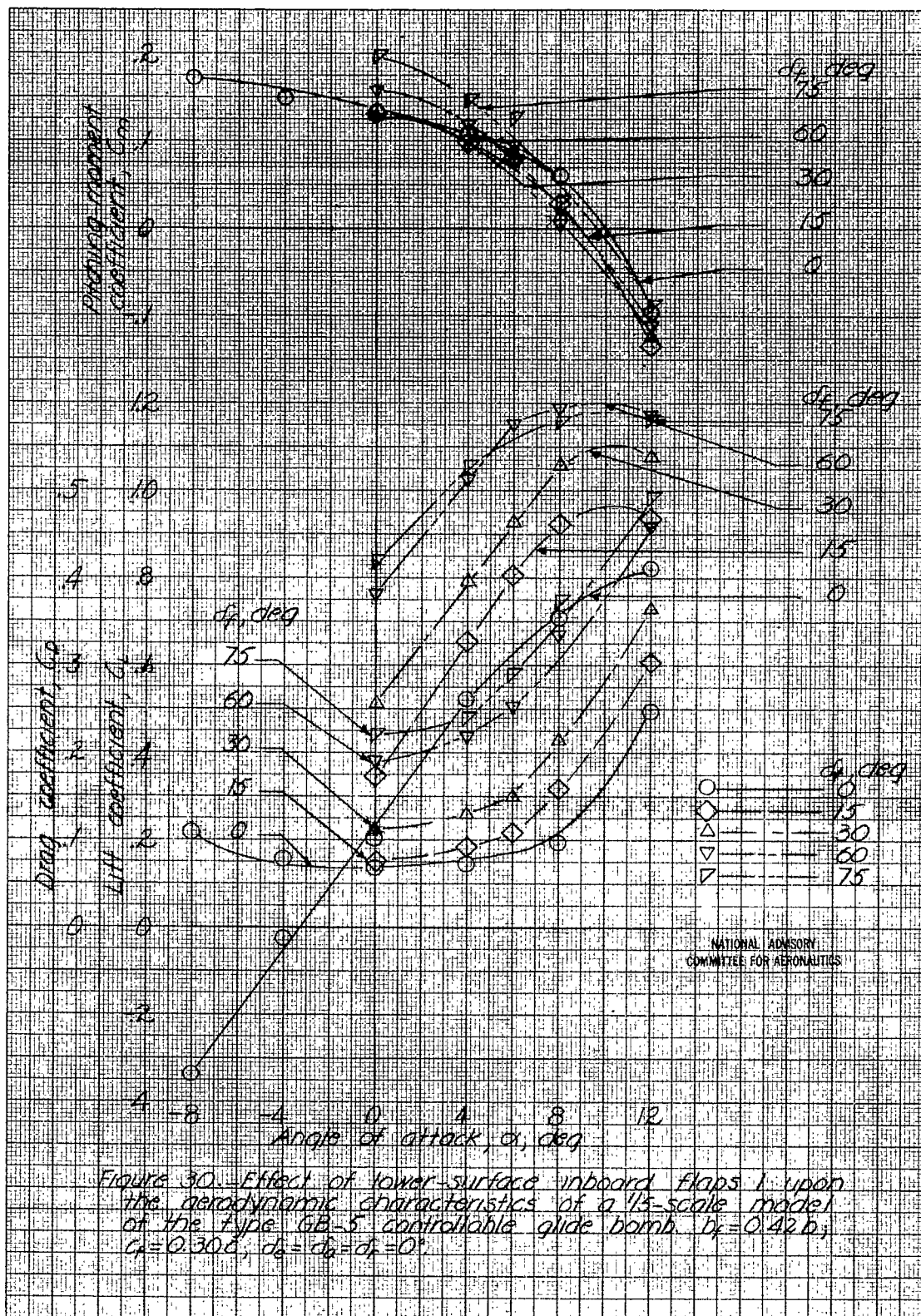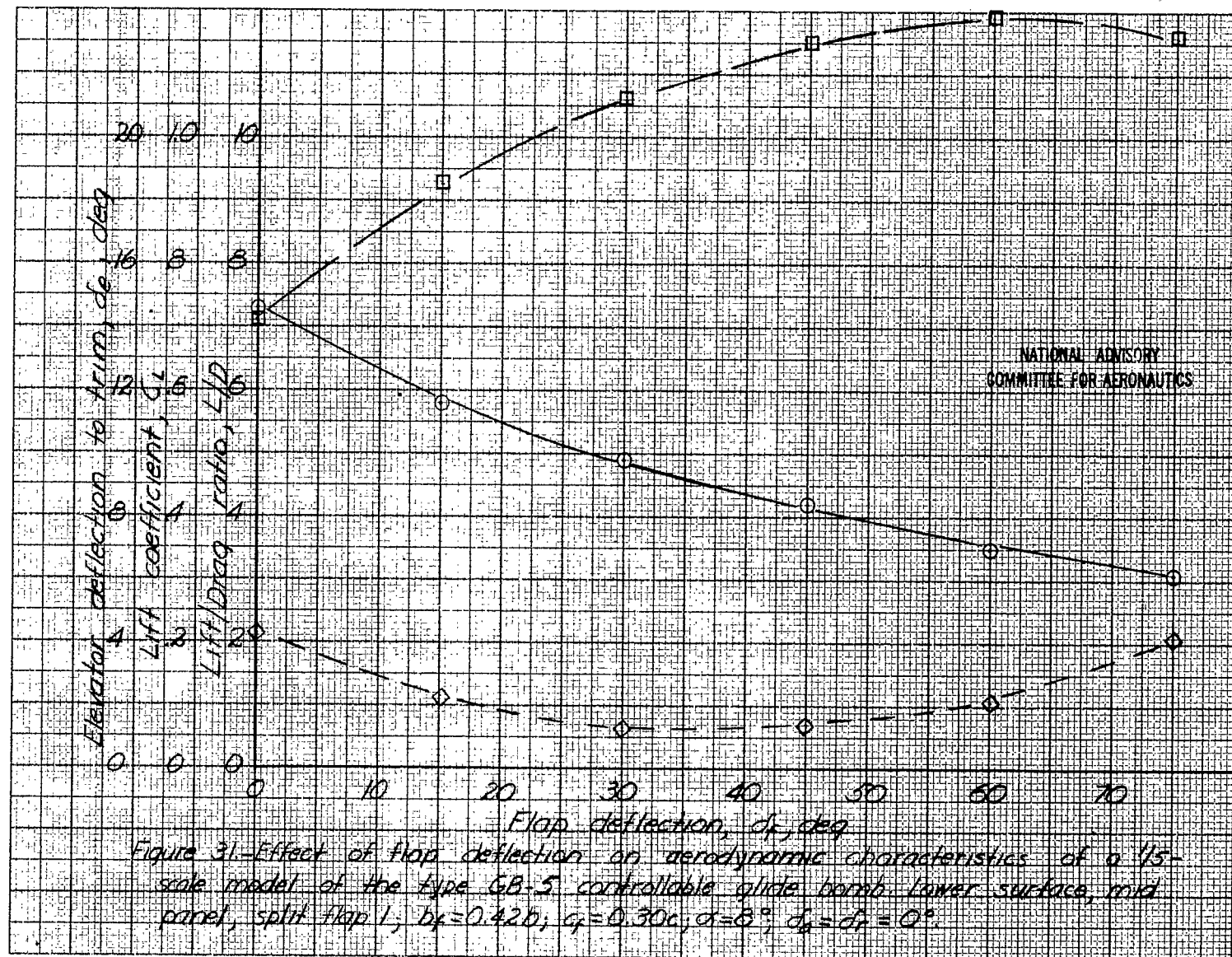
Figure 30.- Effect of lower-surface inboard flaps I upon the aerodynamic characteristics of a 1/5-scale model of the type GB-5 controllable glide bomb. $b_f=0.42\,b$; $c_f=0.30\,c$; $d_e=d_g=d_r=0°$.

Figure 31.-Effect of flap deflection on aerodynamic characteristics of a 1/5-scale model of the type GB-5 controllable glide bomb. Lower surface, mid panel, split flap 1, $b_f=0.42b$; $c_f=0.30c$; $\alpha=8°$; $\delta_e=\delta_r=0°$.
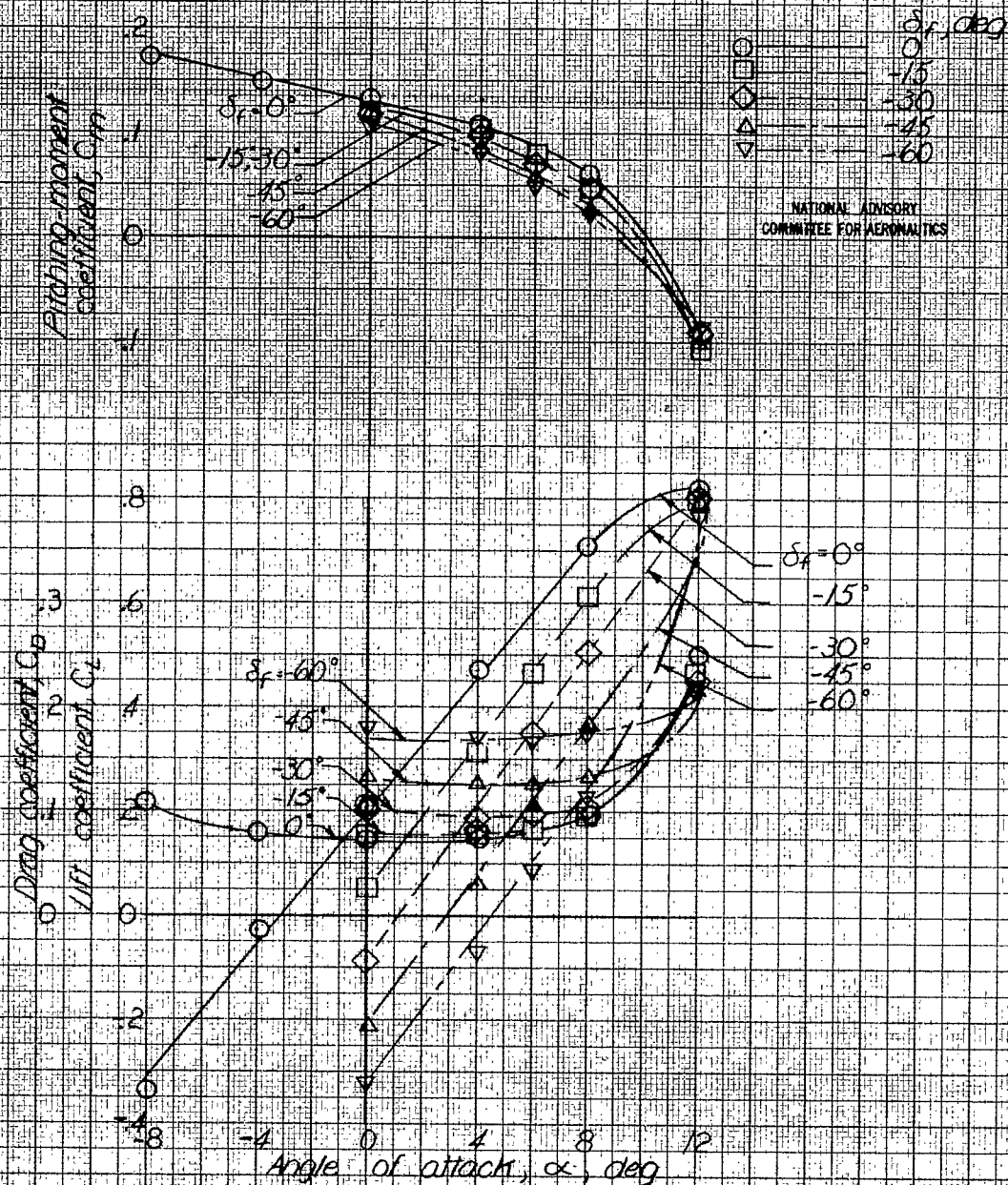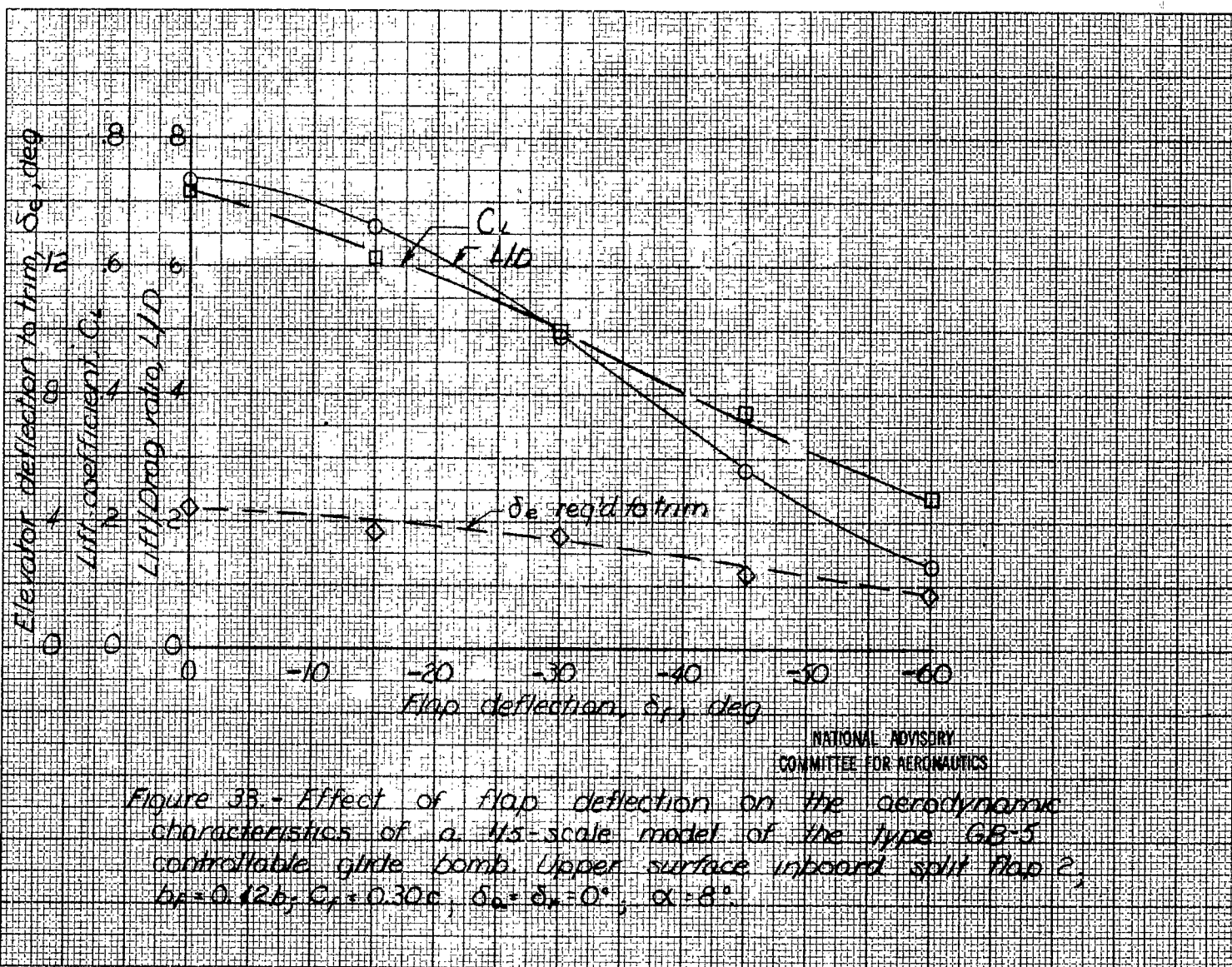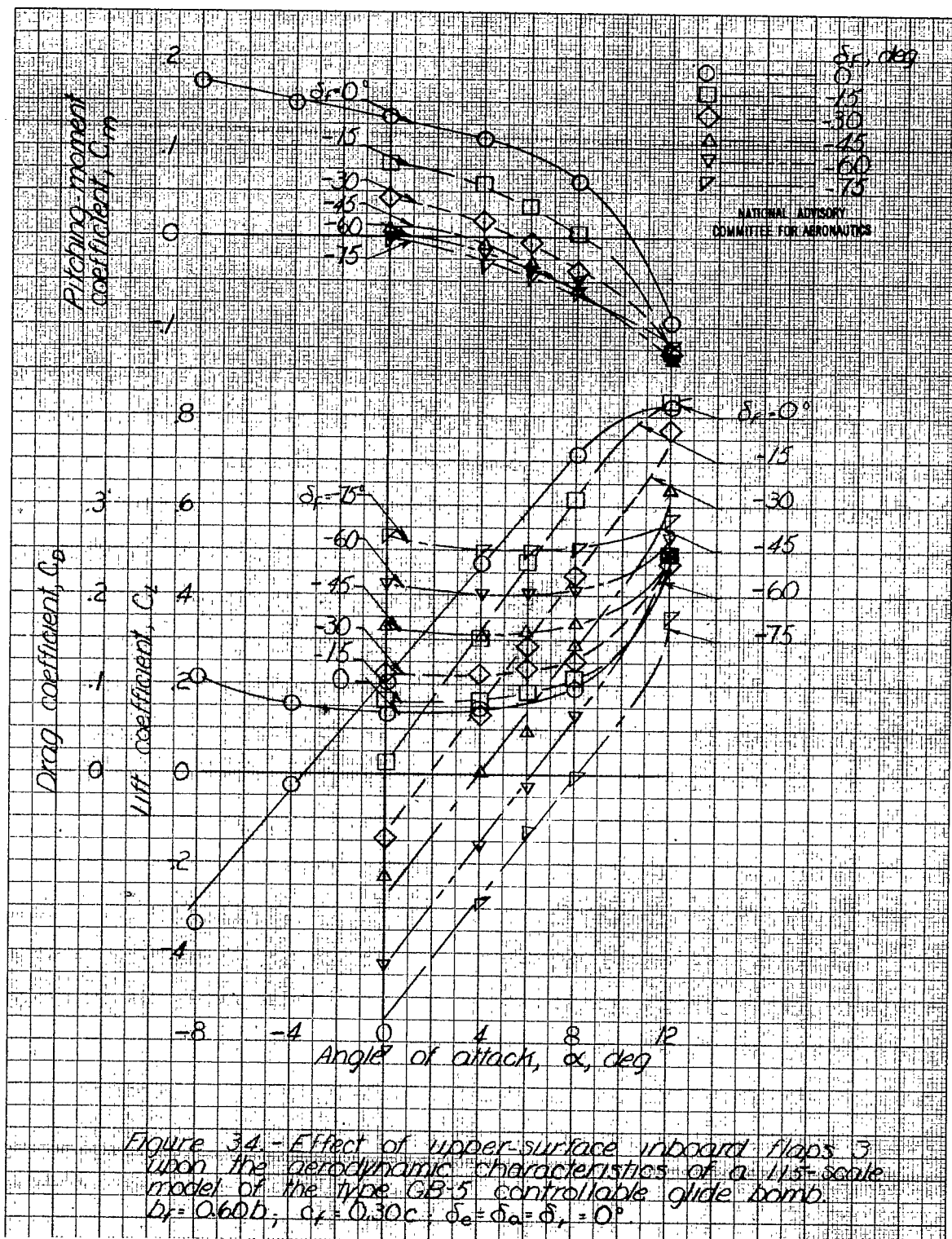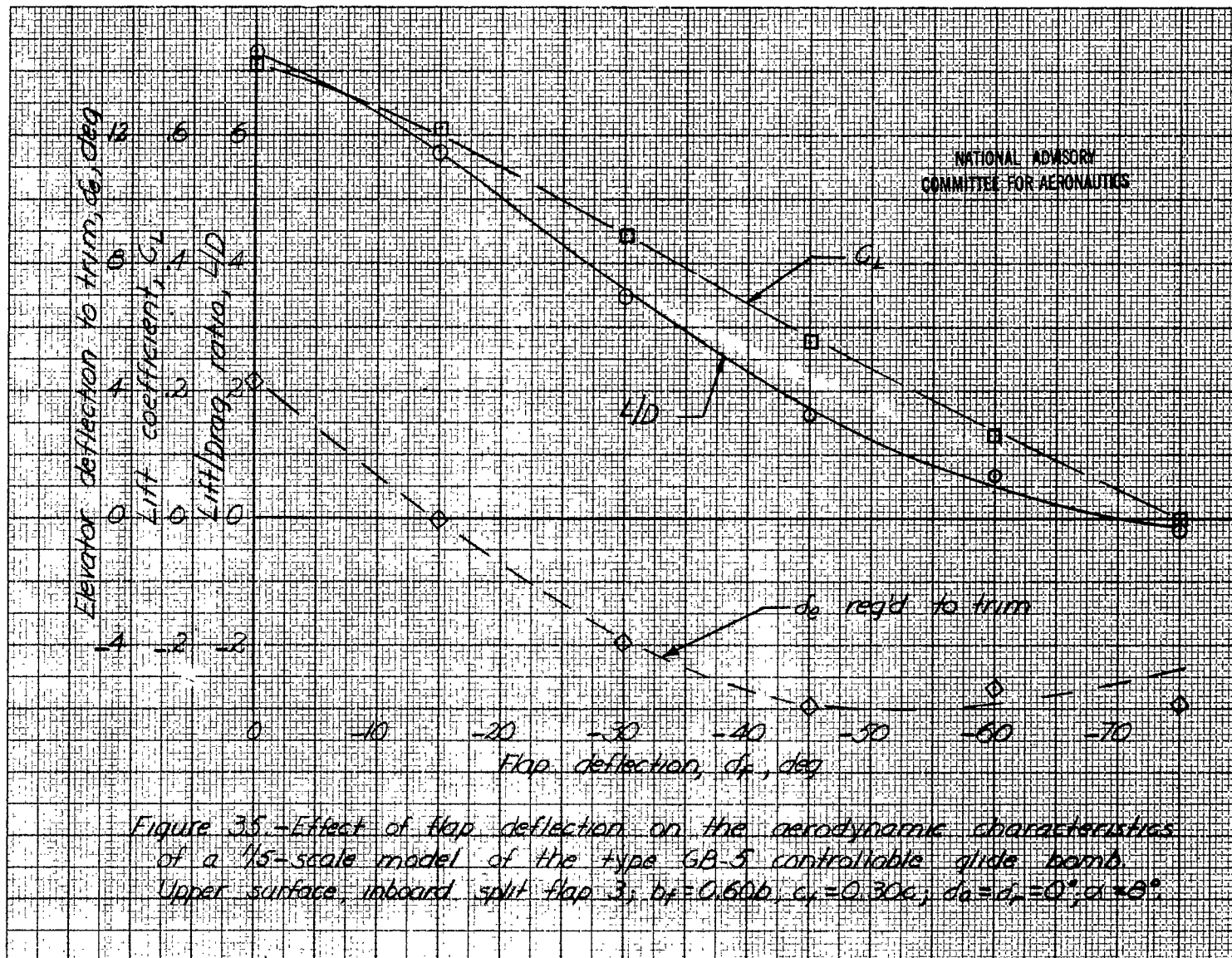
Figure 32.- Effect of upper-surface inboard flaps 2 upon the aerodynamic characteristics of a 1/5-scale model of the type GB-5 controllable glide bomb. $\delta_f = 42^\circ$, $C_f = .30c$, $\delta_e = \delta_a = \delta_r = 0^\circ$.

Figure 33.- Effect of flap deflection on the aerodynamic characteristics of a 1/5-scale model of the type GB-5 controllable glide bomb. Upper surface inboard split flap 2, $b_f = 0.12b$; $C_f = 0.30c$, $\delta_a = \delta_r = 0°$, $\alpha = 8°$.
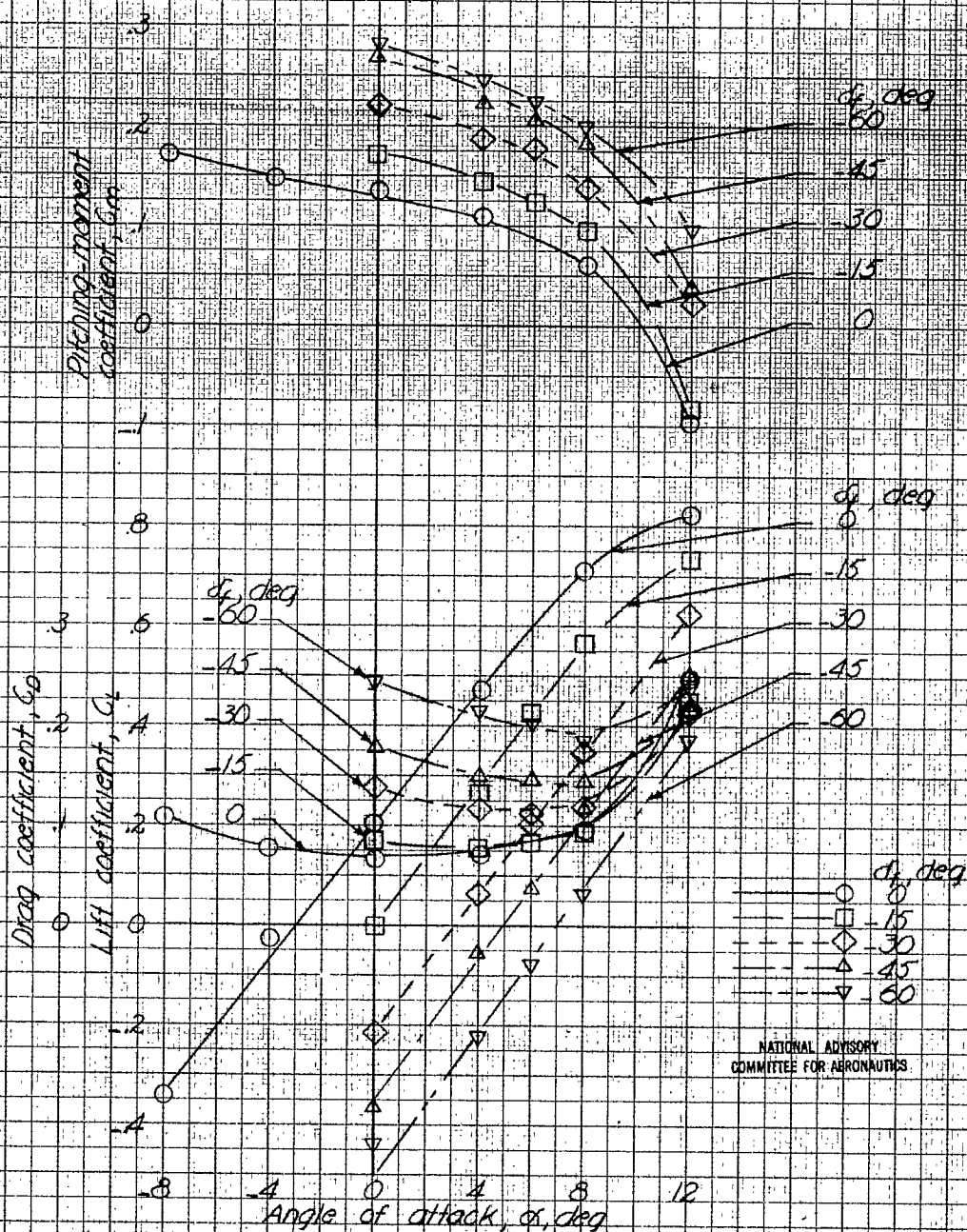
Figure 34.- Effect of upper-surface inboard flaps 3 upon the aerodynamic characteristics of a 1/15-scale model of the type GB-5 controllable glide bomb. $b_f = 0.60b$; $c_f = 0.30c$; $\delta_e = \delta_a = \delta_r = 0°$.

Figure 35.- Effect of flap deflection on the aerodynamic characteristics of a 1/5-scale model of the type GB-5 controllable glide bomb. Upper surface, inboard split flap 3; $b_f = 0.60b$, $c_f = 0.30c$; $\delta_a = \delta_r = 0°; \alpha = 8°$.

Figure 36.- Effect of upper-surface outboard flaps 4 upon the aerodynamic characteristics of a 1/5-scale model of the type GB-5 controllable glide bomb. $b_f = 0.60b$; $c_f = 0.30c$; $d_e = d_a = d_r = 0°$
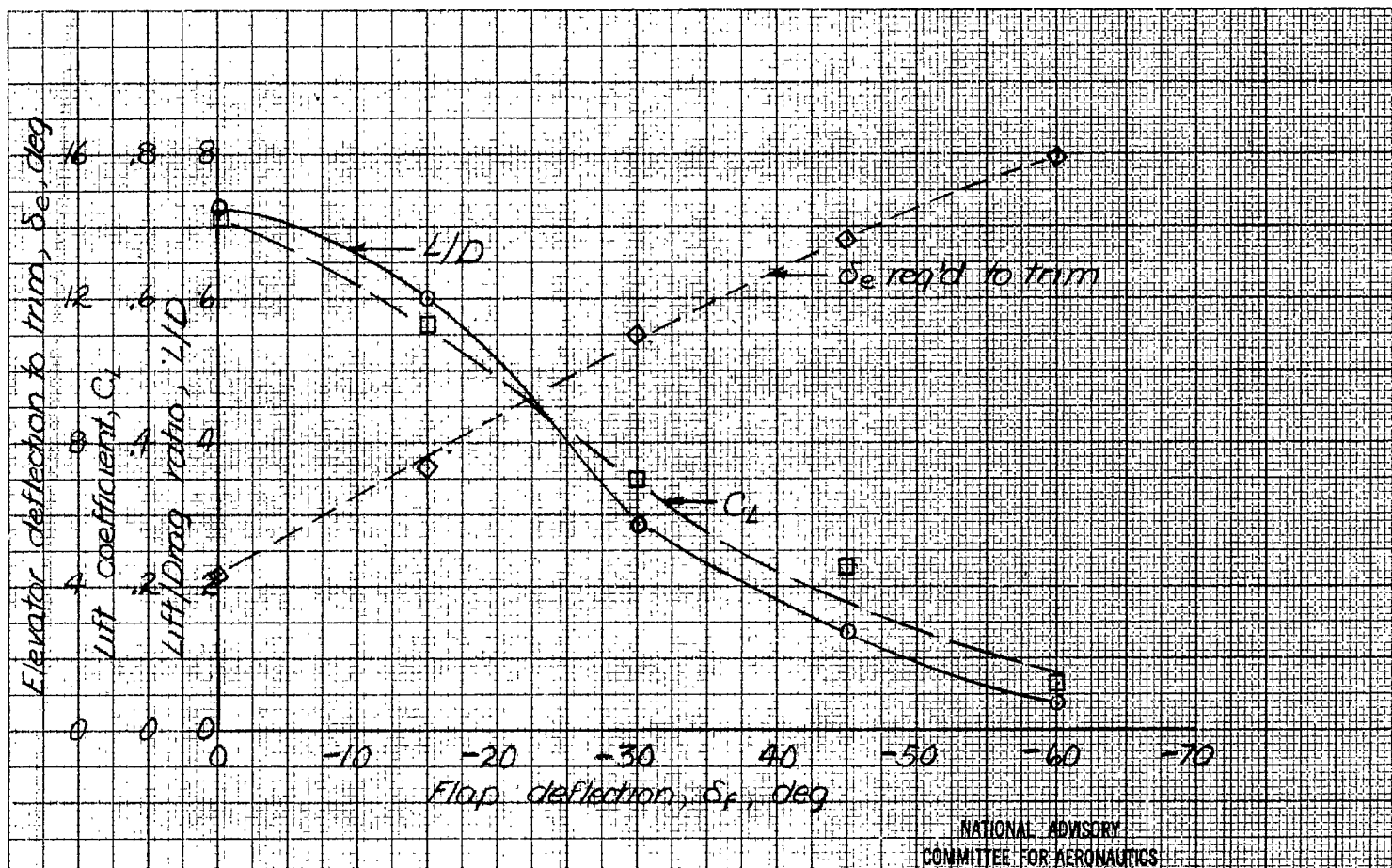
Figure 37.- Effect of flap deflection on the aerodynamic characteristics of a 1/5-scale model of the type GB-5 controllable glide bomb. Upper-surface, outboard split flap 4; $b_f = 0.60b$; $c_f = 0.30c$; $\delta_a = \delta_r = 0$, $\alpha = 8°$.
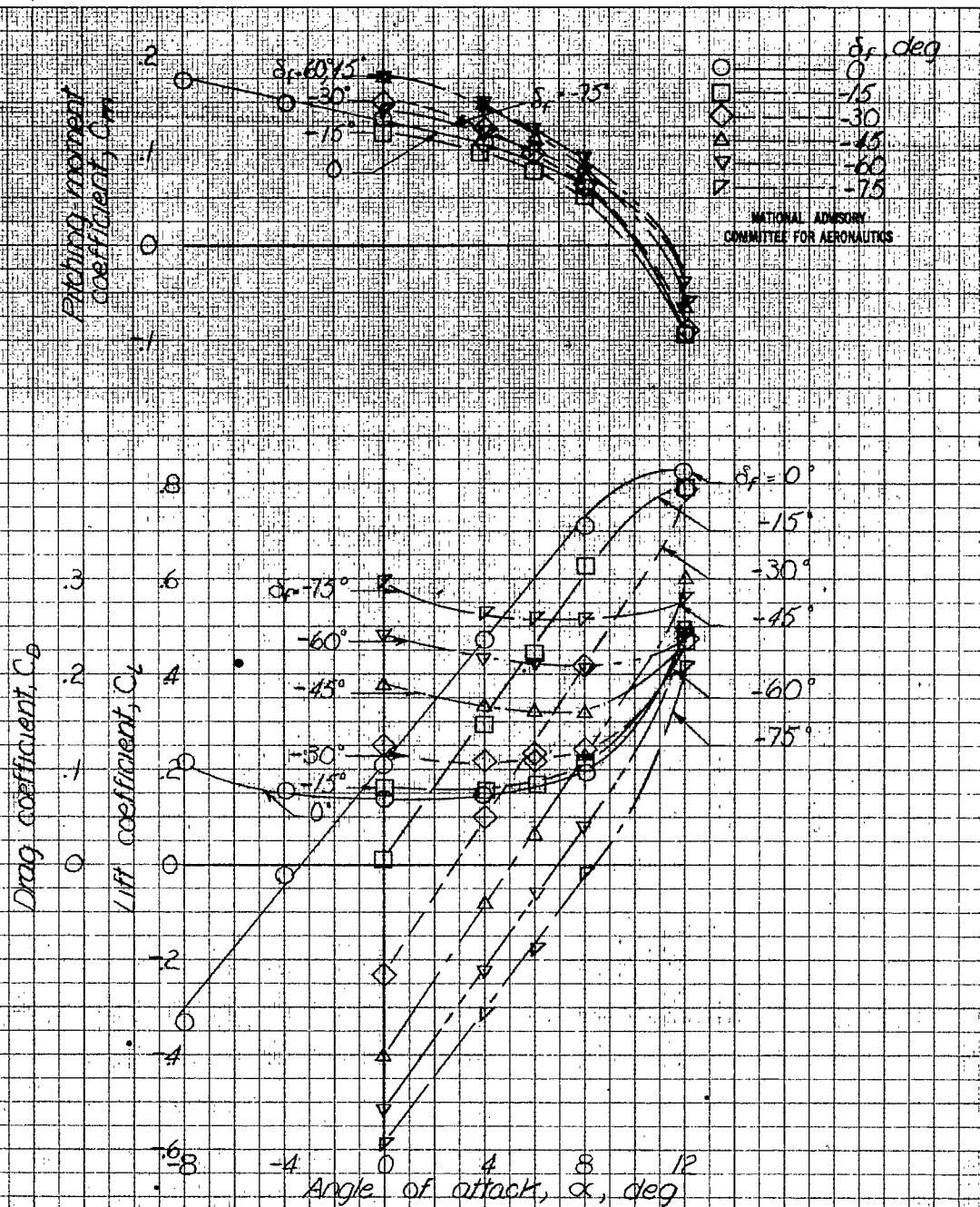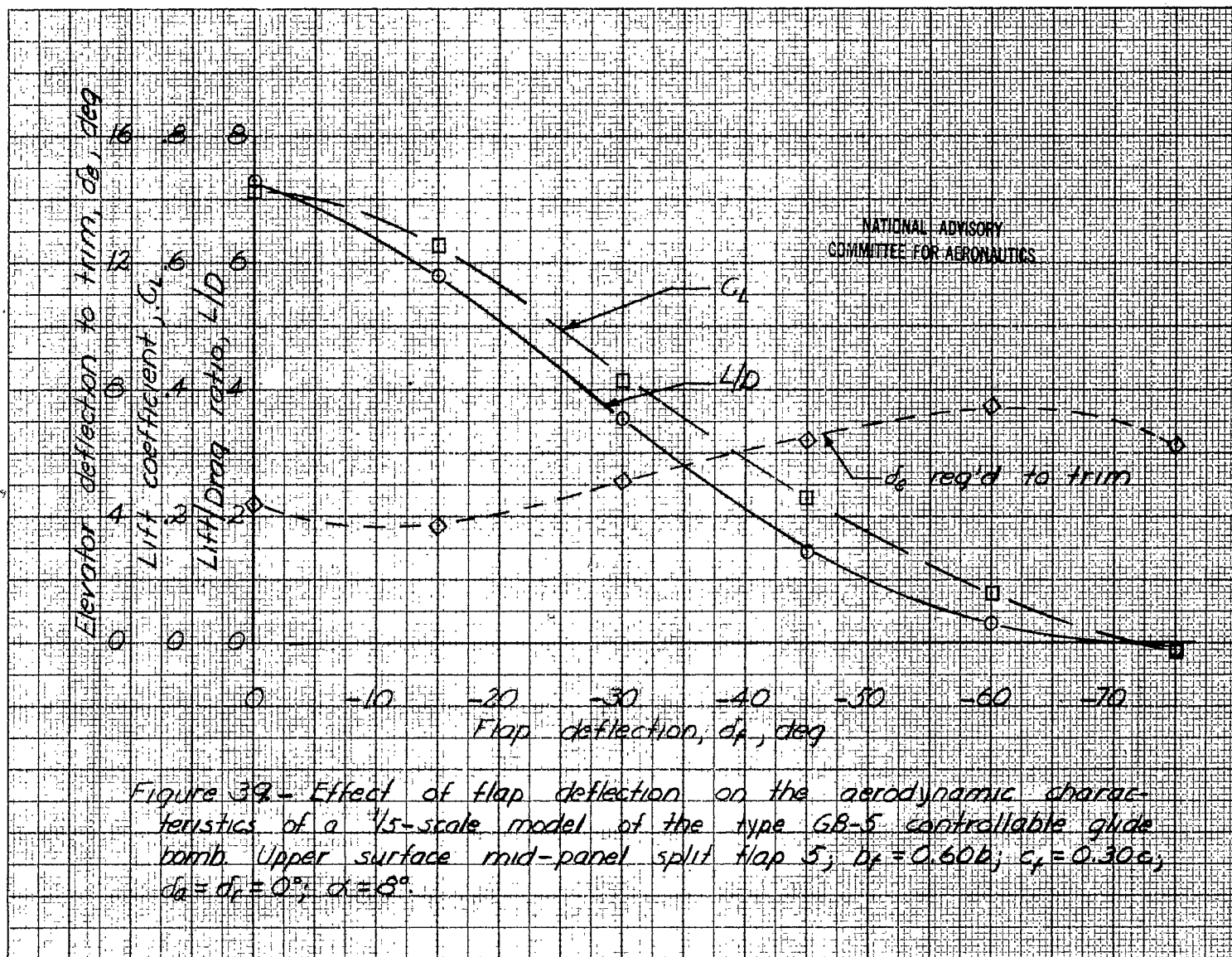
Figure 38.- Effect of upper-surface flaps δ upon the aerodynamic characteristics of a 1/5-scale model of the type GB-5 controllable glide bomb. $b_f = 0.60b$; $C_f = 0.30c$; $\delta_e = \delta_a = \delta_r = 0°$.

Figure 39.– Effect of flap deflection on the aerodynamic characteristics of a 1/5-scale model of the type GB-5 controllable glide bomb. Upper surface mid-panel split flap 5; $b_f = 0.60b$; $c_f = 0.30c$; $d_a = d_r = 0°$; $\alpha = 8°$.